

---

# Nonparametric Filtering, Estimation and Classification using Neural Jump ODEs

**Jakob Heiss**

*Department of Mathematics  
ETH Zurich  
Department of Statistics  
UC Berkeley*

*[jakob.heiss@berkeley.edu](mailto:jakob.heiss@berkeley.edu)*

**Florian Krach**

*Department of Mathematics  
ETH Zurich*

*[florian.krach@math.ethz.ch](mailto:florian.krach@math.ethz.ch)*

**Thorsten Schmidt**

*Department of Mathematics  
Albert-Ludwigs-Universität Freiburg*

*[thorsten.schmidt@stochastik.uni-freiburg.de](mailto:thorsten.schmidt@stochastik.uni-freiburg.de)*

**Félix B. Tambe-Ndonfack**

*Department of Mathematics  
Albert-Ludwigs-Universität Freiburg*

*[felix.ndonfack@stochastik.uni-freiburg.de](mailto:felix.ndonfack@stochastik.uni-freiburg.de)*

## Abstract

Neural Jump ODEs model the conditional expectation between observations by neural ODEs and jump at arrival of new observations. They have demonstrated effectiveness for fully data-driven online forecasting in settings with irregular and partial observations, operating under weak regularity assumptions (Herrera et al., 2021; Krach et al., 2022). This work extends the framework to input-output systems, enabling direct applications in online filtering and classification. We establish theoretical convergence guarantees for this approach, providing a robust solution to  $L^2$ -optimal filtering. Empirical experiments highlight the model's superior performance over classical parametric methods, particularly in scenarios with complex underlying distributions. These results emphasize the approach's potential in time-sensitive domains such as finance and health monitoring, where real-time accuracy is crucial.

## 1 Introduction

Time series analysis is important in many fields, such as meteorology, climate science, economics, finance, health care, medicine and more. The probably most important, but at the same time also most challenging, tasks are forecasting (or estimation), filtering, and classification of time series data, in particular when done *online*, i.e., incorporating new observations directly upon their arrival. Classically, parametric approaches were used for these tasks, where certain models with a few interpretable parameters were assumed such that the analysis could be done analytically. In contrast to this, fully data-driven machine learning (ML) approaches have recently become more important due to their excellent empirical performance. One class of these approaches is based on neural networks, using so many parameters that they can effectively be called nonparametric. They are highly flexible and offer theoretical guarantees through their universal approximation property.

Recurrent neural networks (RNNs) (Rumelhart et al., 1985; Jordan, 1997) are the most prominent approaches for time series. However, they are limited to regular, equidistant observations without missing values. In this work we focus on neural jump ODEs (NJ-ODEs), introduced in Herrera et al. (2021) and refined in Krach

---

et al. (2022); Andersson et al. (2024); Krach & Teichmann (2024). This approach is highly suited for time series estimation and is able to work with irregularly and incompletely observed data. Although adaptations for filtering were already proposed in Krach et al. (2022), their main and natural application area is online *forecasting*, where discrete and potentially incomplete past observations of a continuous-time process  $X$  are used to optimally *estimate* future values of this process  $X$ . In particular, the assumption for NJ-ODEs has so far been that the *output process*  $V$  (i.e., the process to be estimated) coincides with the *input process*  $U$  (i.e., the process which is (partially) observed and used as input to the model). In this work, we generalize the framework to online *filtering* of input-output systems, called input-output NJ-ODE (IO NJ-ODE) in the following.

Applications of the approach are classical stochastic filtering (with discrete observations), filtering with partial and irregular observations and parameter filtering in addition to forecasting. Moreover, the proposed input-output configuration is applicable to online *classification*, where arbitrary features can be used as input  $U$  to predict conditional class probabilities. Since it can process sequential, real-time data inputs and continually generates predictions based on the most up-to-date information, the framework can be applied efficiently in time-sensitive domains like financial market analysis or health monitoring systems, where input-output relationships are central to decision making.

## 1.1 Contribution

When input and output processes  $U$  and  $V$  coincide, the setting of Krach et al. (2022) is recovered. Otherwise, the IO NJ-ODE proposed in this work constitutes a targeted approach for the filtering task. We provide a thorough theoretical framework for the general input-output setting and give minimal assumptions (Section 2) to prove convergence (Section 4) of our IO NJ-ODE model (Section 3) to the conditional expectation, which is the  $L^2$ -optimal solution to the filtering and estimation problem. To establish these theoretical guarantees, we need to introduce a new objective function adapted to the input-output setting. In Section 7, we compare the original and this new objective function and discuss which one should be used depending on the task at hand. Several examples for which our model can be applied are given in Section 5. Besides classical stochastic filtering, we put a special focus on parameter filtering, where the parameters  $\alpha$  of a stochastic process  $X^\alpha$  should be estimated from observations of  $X^\alpha$ . Moreover, we discuss that online classification tasks fall into our framework, by choosing the indicators for each class label as output process  $U$ . Several experiments are provided in Section 6. For clarity and ease of reading and comprehension, we build on the setting in Krach et al. (2022), but note that the extensions to a dependent observation framework, noisy observations and long-term predictions can equivalently be incorporated as described in Andersson et al. (2024); Krach & Teichmann (2024).

## 1.2 Related Work

As mentioned before, this work is based on the Neural Jump ODE literature that started with Herrera et al. (2021) and was lifted to a new level of generality in Krach et al. (2022). The extensions of Andersson et al. (2024); Krach & Teichmann (2024) are conceptually parallel developments to this work, both building on Herrera et al. (2021). The ideas of these 3 works should be understood as building blocks that can be stacked together as desired. This concept is realized in our implementation (available at <https://github.com/FlorianKrach/PD-NJODE>). For more related work on the background of Neural Jump ODEs, we refer the interested reader to Herrera et al. (2021); Krach et al. (2022); Andersson et al. (2024).

In this work, we use particle filters (Djuric et al., 2003) as baseline method to approximate the true conditional expectation when no analytic expression is available for it. In contrast to our model which is fully data-driven, classical particle filters need full knowledge of the underlying distributions to be applicable. Deep learning extensions of particles filters (Maddison et al., 2017; Le et al., 2017; Corenflos et al., 2021; Lai et al., 2022) provide more flexible approaches where the distributions can be learned; however, they are usually restricted to discrete state space models with regular and complete observations, while our method naturally deals with random (and therefore irregular) observation times and missing values. Deep learning extensions of the Kalman filter, like KalmanNet (Revach et al., 2022) or Deep Kalman Filters (Krishnan et al., 2015), as well as related works (Karl et al., 2016; Naesseth et al., 2018; Archer et al., 2015; Krishnan et al., 2017) have

similar limitations as deep particle filters. Hence, without adjustments these methods cannot be used as baselines for our model in general settings.

## 2 Problem Setting

In the following we provide a rigorous theoretical framework, which is, for simplicity, based on a combination of [Krach et al. \(2022, Section 2\)](#) and [Andersson et al. \(2024\)](#). Including the extensions for a dependent observation framework, noisy observations and long-term predictions as proposed in [Andersson et al. \(2024\)](#); [Krach & Teichmann \(2024\)](#) is straight forward, following these works.

### 2.1 Stochastic Process, Random Observation Times and Observation Mask

Let  $d = d_U + d_V \in \mathbb{N}$  be the dimension and  $T > 0$  be a fixed time horizon. We work on a filtered probability space  $(\Omega, \mathcal{F}, \mathbb{F}, \mathbb{P})$ , where the filtration  $\mathbb{F} = (\mathcal{F}_t)_{t \in \mathbb{R}_+}$  satisfies the usual conditions, i.e. , the  $\sigma$ -field  $\mathcal{F}$  is  $\mathbb{P}$ -complete,  $\mathbb{F}$  is right-continuous and  $\mathcal{F}_0$  contains all  $\mathbb{P}$ -null sets of  $\mathcal{F}$ . On this filtered probability space, we consider an adapted,  $d$ -dimensional, càdlàg stochastic process  $Z := (Z_t)_{t \in [0, T]}$ . We split  $Z = (U, V)$  into the  $d_U$ -dimensional input process  $U$  and the  $d_V$ -dimensional output process  $V$ . The running maximum process of  $Z$  is defined as

$$Z_t^* := \sup_{0 \leq s \leq t} |Z_s|_1 = \sup_{0 \leq s \leq t} (|U_s|_1 + |V_s|_1), \quad 0 \leq t \leq T.$$

We denote the set of random times where the output process jumps by  $\mathcal{J} = \{(\omega, t) : \Delta V_t(\omega) \neq 0\}$ , with  $\Delta V_t := V_t - V_{t-}$ .

In addition to the input-output process, we consider an exogenous observation *masking*, which captures if a coordinate of  $Z$  is masked and therefore excluded from the data set. We assume that a random number of  $n \in \mathbb{N}$  observations take place at the random times

$$0 = t_0 < t_1 < \dots < t_n \leq T$$

and denote by  $\bar{n} = \sup \{k \in \mathbb{N} \mid \mathbb{P}(k = n) > 0\} \in \mathbb{N} \cup \{\infty\}$  the maximal value of  $n$ . Note that this setup is extremely flexible and allows, in particular, a possibly unbounded number of observations in the finite time interval  $[0, T]$ . Moreover, let

$$\tau(t) := \max\{t_k : 0 \leq k \leq n, t_k \leq t\}$$

denote the last observation time (or zero if no observation was made yet) before time  $t \in [0, T]$ . Finally, the observation mask is a sequence of random variables  $M = (M_k)_{0 \leq k \leq \bar{n}}$  taking values in  $\{0, 1\}^d$ . If  $M_k^j = 1$ , then the  $j$ -th coordinate  $Z_{t_k}^j$  is observed at observation time  $t_k$ . By abuse of notation, we also write  $M_{t_k} := M_k$ . For notational simplicity, we will set  $t_k(\omega) = \infty$  for  $k > n(\omega)$  and for all appearing processes their value at  $t_k = \infty$  to 0.

### 2.2 Information $\sigma$ -algebra

The information available at time  $t$  is given by the values of the input process  $U$  at the observation times when not masked. This leads to the filtration of the currently available information  $\mathbb{A} := (\mathcal{A}_t)_{t \in [0, T]}$  given by

$$\mathcal{A}_t := \sigma(U_{t_i, j}, t_i, M_{t_i} \mid t_i \leq t, j \in \{1 \leq l \leq d_U \mid M_{t_i, l} = 1\}),$$

where  $\sigma(\cdot)$  represents the generated  $\sigma$ -algebra. By the definition of  $\tau$ , we have  $\mathcal{A}_t = \mathcal{A}_{\tau(t)}$  for all  $t \in [0, T]$ . Additionally, for any fixed observation (or stopping) time  $t_k$ , the stopped and pre-stopped<sup>1</sup>  $\sigma$ -algebras at  $t_k$  are

$$\begin{aligned} \mathcal{A}_{t_k} &:= \sigma(U_{t_i, j}, t_i, M_{t_i} \mid i \leq k, j \in \{1 \leq l \leq d_U \mid M_{t_i, l} = 1\}), \\ \mathcal{A}_{t_k-} &:= \sigma(U_{t_i, j}, t_i, M_{t_i}, t_k \mid i < k, j \in \{1 \leq l \leq d_U \mid M_{t_i, l} = 1\}). \end{aligned}$$

<sup>1</sup>The stopped  $\sigma$ -algebra ([Karandikar & Rao, 2018, Definition 2.37](#)) is defined as  $\mathcal{F}_\tau = \{A \in \sigma(\cup_t \mathcal{F}_t) : A \cap \{\tau \leq t\} \in \mathcal{F}_t \forall t\}$ , where  $\tau$  is the stopping time. The pre-stopped  $\sigma$ -algebra ([Karandikar & Rao, 2018, Definition 8.1](#)) is defined as  $\mathcal{F}_{\tau-} = \sigma(\mathcal{F}_0 \cup \{A \cap \{t < \tau\} : A \in \mathcal{F}_t, t < \infty\})$ , where  $\tau$  is the stopping time.

## 2.3 Notation and Assumptions on the Stochastic Process $Z$

Since we are working with an input-output system, we are interested in the conditional expectation of the output process  $V$ , given the observation of the input process (collected in the information  $\sigma$ -algebra), denoted as  $\hat{V} = (\hat{V}_t)_{0 \leq t \leq T}$  and defined via

$$\hat{V}_t := \mathbb{E}[V_t | \mathcal{A}_t].$$

We define the interpolation of the observations of  $\bar{U} := (U_t, \tilde{n}_t, t)_{t \in [0, T]}$  made until time  $t$ , where  $\tilde{n}_t := (\sum_k M_{k,j} \mathbb{1}_{t_k \leq t})_{1 \leq j \leq d_U}$  counts the coordinate-wise observations, by  $\tilde{U}^{\leq t}$  for any  $0 \leq t \leq T$ . At time  $0 \leq s \leq T$ , its  $j$ -th coordinate is given by

$$\tilde{U}_{s,j}^{\leq t} := \begin{cases} \bar{U}_{t_{a(s,t,j),j}} \frac{t_{b(s,t,j),j} - s}{t_{b(s,t,j),j} - t_{b(s,t,j),j-1}} + \bar{U}_{t_{b(s,t,j),j}} \frac{s - t_{b(s,t,j),j-1}}{t_{b(s,t,j),j} - t_{b(s,t,j),j-1}}, & \text{if } t_{b(s,t,j),j-1} < s \leq t_{b(s,t,j),j}, \\ \bar{U}_{t_{a(s,t,j),j}}, & \text{if } s \leq t_{b(s,t,j),j-1}, \end{cases}$$

where

$$\begin{aligned} a(s, t, j) &:= \max\{0 \leq a \leq n \mid t_a \leq \min(s, t), M_{t_a, j} = 1\}, \\ b(s, t, j) &:= \inf\{1 \leq b \leq n \mid s \leq t_b \leq t, M_{t_b, j} = 1\}, \end{aligned}$$

letting  $t_\infty := T$  and  $\inf \emptyset := \infty$ . Then,  $\tilde{U}^{\leq t}$  is a continuous version (without information leakage and with time-consistency) of the rectilinear (“forward fill”) interpolation of the observations. According to this definition,  $\tilde{U}^{\leq \tau(t)}$  is measurable with respect to  $\mathcal{A}_{\tau(t)}$  for any  $t$ , and for any  $r \geq t$  and  $s \leq \tau(t)$ , we have  $\tilde{U}_s^{\leq \tau(t)} = \tilde{U}_s^{\leq \tau(r)}$ . Clearly, the paths of  $\tilde{U}^{\leq \tau(t)}$  belong to  $BV^c([0, T])$ , the set of continuous  $\mathbb{R}^{d_U}$ -valued paths of bounded variation on  $[0, T]$  (cf. Definition A.2).

We note that the Doob-Dynkin Lemma (Kallenberg, 2021, Lemma 1.14) implies the existence of measurable functions  $F_j : [0, T] \times [0, T] \times BV^c([0, T]) \rightarrow \mathbb{R}$  such that  $\hat{V}_{t,j} = F_j(t, \tau(t), \tilde{U}^{\leq \tau(t)})$ .

For the remainder of this article, we will assume that the following set of assumptions holds throughout. Those are a maximally weakened version of the assumptions made in Krach et al. (2022).

**Assumption 1.** *We assume that the input process  $U$  is fully observed at  $t_0 = 0$ . Moreover, we assume that for every  $1 \leq k, l \leq \bar{n}$ ,  $M_k$  is independent of  $t_l$  and of  $n$  and  $\mathbb{P}(M_{k,j} = 1) > 0$  for all  $d_U + 1 \leq j \leq d$  on the training set (during training, every coordinate of the output process  $V$  can be observed with positive probability at any observation time).*

**Assumption 2.** *Almost surely  $V$  is not observed at a jump, i.e.,  $\mathbb{P}(\{t_j \in \mathcal{J} \mid j \leq n\}) = \mathbb{P}(\{\Delta V_{t_j} \neq 0 \mid j \leq n\}) = 0$ .*

**Assumption 3.**  *$F_j$  are continuous and differentiable in their first coordinate  $t$  such that their partial derivatives with respect to  $t$ , denoted by  $f_j$ , are again continuous and the following integrability condition holds*

$$\mathbb{E} \left[ \frac{1}{n} \sum_{i=1}^n (|F_j(t_i, t_i, \tilde{U}^{\leq t_i})|^2 + |F_j(t_{i-1}, t_{i-1}, \tilde{U}^{\leq t_{i-1}})|^2) + \int_0^T |f_j(t, \tau(t), \tilde{U}^{\leq \tau(t)})|^2 dt \right] < \infty. \quad (1)$$

**Assumption 4.**  *$U^*$  is  $L^2$ -integrable, i.e.,  $\mathbb{E}[(U_T^*)^2] < \infty$ , and  $\mathbb{E} \left[ \frac{1}{n} \sum_{i=1}^n V_{t_i}^2 \right] < \infty$ .*

**Assumption 5.** *The random number of observations  $n$  is integrable, i.e.,  $\mathbb{E}[n] < \infty$ .*

**Assumption 6.** *The process  $X$  is independent of the observation framework consisting of the random variables  $n, (t_i, M_i)_{i \in \mathbb{N}}$ .*

**Remark 2.1.** *The probability that any two observation times are closer than  $\epsilon > 0$  converges to 0 when  $\epsilon$  does, i.e., if  $\delta_{\min}(\tilde{\omega}) := \min_{0 \leq i \leq n(\tilde{\omega})} |t_{i+1}(\tilde{\omega}) - t_i(\tilde{\omega})|$  then  $\lim_{\epsilon \rightarrow 0} \mathbb{P}(\delta_{\min} < \epsilon) = 0$ . This is equivalent to  $\mathbb{P}(\delta_{\min} = 0) = 0$ , which is satisfied when the observation times are strictly increasing.*

**Remark 2.2.** *Assumption 1 can easily be generalized to settings where  $U_0$  is only partly or not observed (see Krach et al., 2022, Remark 2.2). Furthermore, the assumption that all coordinates can be observed at any observation time can be weakened as shown in Section 4.3.*

---

**Remark 2.3.** Assumption 6 puts us in the same setting as was hard-coded through the product probability space in Krach et al. (2022). Moreover, the independence Assumptions 1 and 6 can easily be replaced by conditional independence assumptions as formulated in Andersson et al. (2024, Section 4).

As shown in Krach et al. (2022, Proposition 2.5) and also implied by Lemma 4.1, the conditional expectation process  $\hat{V}$  is the optimal process in  $L^2(\Omega, \mathbb{A}, \mathbb{P})$  approximating  $(V_t)_{t \in [0, T]}$  and it is unique up to  $\mathbb{P}$ -null-sets.

Throughout this paper, we will use the following distance functions (based on the observation times) between processes and define indistinguishability with them. This is a slight modification for the present setting from the corresponding definition in Krach et al. (2022). The proposed pseudo metric controls on the one side the prediction before the jump at  $t_k$  and on the other side the realized jump size.

**Definition 2.4.** Fix  $r \in \mathbb{N}$  and set  $c_0(k) := (\mathbb{P}(n \geq k))^{-1}$ . The family of (pseudo) metrics  $d_k$ ,  $1 \leq k \leq \bar{n}$ , for two càdlàg  $\mathbb{A}$ -adapted processes  $\eta, \xi : [0, T] \times \Omega \rightarrow \mathbb{R}^r$  is defined as

$$d_k(\eta, \xi) = c_0(k) \mathbb{E} \left[ \mathbf{1}_{\{k \leq n\}} (|\eta_{t_k} - \xi_{t_k}|_1 + |\eta_{t_k} - \xi_{t_k}|_1) \right]. \quad (2)$$

We call the processes indistinguishable at observation points, if  $d_k(\eta, \xi) = 0$  for every  $1 \leq k \leq \bar{n}$ .

The motivation for this distance is that we can only approximate the target process  $V$  at times, where we can potentially observe it. In particular, if  $V$  is never observed within a certain time interval, i.e., all observation times have probability 0 to lie within this interval, then it is impossible to learn the dynamics of  $V$  within this time interval. It is important to note that observations of the target process  $V$  (and hence Assumption 1) are only needed for the training of the model, while inference works solely based on the observations of the input process  $U$ . Furthermore it seems important to stress that, since observation times are random and expectations are taken, *all possible* observation times are taken into account in the above definition when indistinguishability is considered.

### 3 The Neural Jump ODE Model for Input-Output Processes

We want to model the relationship between an input process  $U$  and an output process  $V$ , which may have different dimensions and exhibit complex dynamics. More precisely, we want to approximate the functions  $F_j$ , which map the observations of  $U$  to the optimal prediction of  $V$ . To achieve this, we define the Input-Output Neural Jump ODE (IO NJ-ODE) model, which leverages neural networks to capture the underlying structure of these processes. Below, we outline the IO NJ-ODE model definition, incorporating the necessary modifications to the original framework define by Krach et al. (2022).

One key component of the model is the truncated signature. The intuition to rely on signatures is the following: since the path of  $X$  can be reconstructed from its signature, any statistic, being a function of the path, can equivalently be represented as a function of the signature. The truncated signature contains the typically most relevant information up to the order  $m$  and therefore serves as a tractable approximation of path information. More precisely, let  $I$  denote a compact interval in  $\mathbb{R}$  and  $X : I \rightarrow \mathbb{R}^\delta$  be a continuous path with finite variation. The truncated signature transforms this path  $X$  into a finite-dimensional feature vector  $\pi_m(X)$ , i.e., the first  $m + 1$  terms (levels) of the signature of  $X$  (see Appendix A for more details). A well-known result in stochastic analysis states that continuous functions of finite variation paths can be uniformly approximated using truncated signatures. We will require a generalization of this result which allows for an additional, finite-dimensional input, which was proven in Krach et al. (2022, Proposition 3.8). For clarity, we provide the result and details in the Appendix in Proposition A.5.

We introduce, following Krach et al. (2022), Definition 3.12, a special class of neural networks with bounded outputs derived from any set of neural networks.

**Definition 3.1.** Define for dimension  $\delta \in \mathbb{N}$  the Lipschitz continuous and bounded output activation function  $\Gamma_\gamma$  with trainable parameter  $\gamma > 0$  by

$$\Gamma_\gamma : \mathbb{R}^\delta \rightarrow \mathbb{R}^\delta, x \mapsto x \cdot \min \left( 1, \frac{\gamma}{|x|_2} \right)$$

and the class of bounded output neural networks by

$$\mathcal{N} := \{f_{(\tilde{\theta}, \gamma)} := \Gamma_\gamma \circ \tilde{f}_{\tilde{\theta}} \mid \gamma > 0, \tilde{f}_{\tilde{\theta}} \in \tilde{\mathcal{N}}\},$$

where  $\tilde{\mathcal{N}}$  can be any set of neural networks. We use the notation  $\tilde{f}_{\tilde{\theta}} \in \tilde{\mathcal{N}}$  and  $f_\theta \in \mathcal{N}$  for  $\theta = (\tilde{\theta}, \gamma)$  to highlight the trainable weights  $\tilde{\theta}$  (and  $\gamma$ ) of the respective (bounded output) neural networks.

The key property of the truncation function  $\Gamma_\gamma$  is that  $\Gamma_\gamma(x) = x$  for all  $x$  with  $|x|_2 \leq \gamma$ .

In the following, we consider  $\tilde{\mathcal{N}}$  to be the class of feed-forward neural networks that use Lipschitz continuous activation functions. This implies that for any natural numbers  $d_1, d_2$  and for any compact set  $\mathcal{X} \subset \mathbb{R}^{d_1}$ , the set  $\tilde{\mathcal{N}}$  is a dense subset of the set of continuous functions  $C(\mathcal{X}, \mathbb{R}^{d_2})$  in terms of the supremum norm. Moreover, we assume that all affine functions and, in particular, the identity are in  $\tilde{\mathcal{N}}$ . Recall that  $\pi_m$  is the truncated signature of order  $m$ .

To the (random) observation times  $t_1, \dots, t_n$  we associate the pure-jump process

$$J_t := \sum_{i=1}^n 1_{[t_i, \infty)}(t), \quad 0 \leq t \leq T,$$

which simply counts the observations until the current time  $t$ . Very useful is that the increment  $dJ_t$  either vanishes or equals  $\Delta J_t = 1$  (since we assumed that the observation times are *strictly* increasing), which guarantees a high tractability of the following model class.

**Definition 3.2** (IO NJ-ODE). *The Input-Output Neural Jump ODE model is given by*

$$\begin{aligned} H_0 &= \rho_{\theta_2}(0, 0, \pi_m(0), U_0), \\ dH_t &= f_{\theta_1}\left(H_{t-}, t, \tau(t), \pi_m(\tilde{U}^{\leq \tau(t)} - U_0), U_0, \tilde{U}_t^*, n_t, \delta_t\right) dt \\ &\quad + \left(\rho_{\theta_2}\left(H_{t-}, t, \pi_m(\tilde{U}^{\leq \tau(t)} - U_0), U_0, \tilde{U}_t^*, n_t, \delta_t\right) - H_{t-}\right) dJ_t, \\ G_t &= \tilde{g}_{\tilde{\theta}_3}(H_t). \end{aligned} \tag{3}$$

$f_{\theta_1}, \rho_{\theta_2} \in \mathcal{N}$  are bounded output feedforward neural networks and  $\tilde{g}_{\tilde{\theta}_3} \in \tilde{\mathcal{N}}$  is a feedforward neural network. They have trainable weights  $\theta = (\theta_1, \theta_2, \tilde{\theta}_3) \in \Theta$ , where  $\theta_i = (\tilde{\theta}_i, \gamma_i)$  for  $i \in \{1, 2\}$  and the set of all potential weights for the NJ-ODE is denoted by  $\Theta$ .

While  $H = H^{\theta_1, \theta_2}$  governs the dynamic evolution of the model, the final output  $G$  is obtained after the application of a (standard) feedforward neural network to  $H$ ,  $G = \tilde{g}_{\tilde{\theta}_3}(H^{\theta_1, \theta_2})$ . To emphasize the dependence of the model output on the trainable parameters and its input, we will also write  $G^\theta(\tilde{U}^{\leq \tau(\cdot)})$ .

### 3.1 Objective Functions

Let  $\mathbb{D}$  represent the collection of all càdlàg processes that take values in  $\mathbb{R}^{d_V}$  and are adapted to the filtration  $\mathbb{A}$ . Define the objective functions  $\Psi : \mathbb{D} \rightarrow \mathbb{R}$  and  $L : \Theta \rightarrow \mathbb{R}$  as

$$\Psi(\eta) := \mathbb{E} \left[ \frac{1}{n} \sum_{i=1}^n |\text{proj}_V(M_i) \odot (V_{t_i} - \eta_{t_i})|_2^2 + |\text{proj}_V(M_i) \odot (V_{t_i} - \eta_{t_{i-}})|_2^2 \right], \tag{4}$$

$$L(\theta) := \Psi(G^\theta(\tilde{U}^{\leq \tau(\cdot)})), \tag{5}$$

where  $\odot$  is the element-wise (Hadamard) product,  $\text{proj}_V$  denotes the projection onto the coordinates corresponding to the output variable  $V$ . We call  $L$  the *theoretical* objective function.

We note that objective functions differ from [Krach et al. \(2022\)](#), since here we square both terms separately. This is indeed a necessary adjustment to establish the same theoretical results in the more general setting of input-output systems. In [Section 7](#), we discuss the different implications of the two definitions in more detail.

For the definition of the *empirical* objective function, we assume to have  $N$  independent realizations of the process  $Z$ , of the observation mask  $M$  and of observation times: let  $Z^{(j)} \sim Z$ ,  $M^{(j)} \sim M$  and  $(n^{(j)}, t_1^{(j)}, \dots, t_{n^{(j)}}^{(j)}) \sim (n, t_1, \dots, t_n)$  be i.i.d random variables or processes, respectively. The training data is a single realization of these. We denote  $G^{\theta, j} := G^\theta(\tilde{U}^{\leq \tau(\cdot), (j)})$ . The empirical objective function  $\hat{L}_N$  equals the Monte Carlo approximation of the loss function with those  $N$  samples, given by

$$\hat{L}_N(\theta) := \frac{1}{N} \sum_{j=1}^N \frac{1}{n^{(j)}} \sum_{i=1}^{n^{(j)}} \left| \text{proj}_V(M_i^{(j)}) \odot \left( V_{t_i^{(j)}}^{(j)} - G_{t_i^{(j)}}^{\theta, j} \right) \right|_2^2 + \left| \text{proj}_V(M_i^{(j)}) \odot \left( V_{t_i^{(j)}}^{(j)} - G_{t_i^{(j)}}^{\theta, j} \right) \right|_2^2, \quad (6)$$

and converges  $\mathbb{P}$ -a.s. to  $L(\theta)$  as  $N \rightarrow \infty$ , according to the law of large numbers (see Theorem 4.4).

## 4 Convergence Guarantees

In this section, we present the main results establishing convergence of the IO NJ-ODE model to the optimal prediction. We begin with the convergence result for the theoretical objective function  $L$ , followed by demonstrating convergence when using its Monte Carlo approximation  $\hat{L}$ , i.e., the implementable loss function. In particular, using either  $L$  or  $\hat{L}$ , we show that the model output  $G^\theta$  converges to the true conditional expectation  $\hat{V}$  in the metrics  $d_k$ . Hence, in the limit, the model output is indistinguishable at observations from  $\hat{V}$ . Importantly, the convergence holds when evaluating the trained model on the training set or on an independent test set (see the proof for more details).

For the proof of the convergence results we follow Krach et al. (2022) and extend their results to our settings.

### 4.1 Convergence of the Theoretical Objective Function $L$

Initially, we recall the easy results of Krach et al. (2022, Lemma 4.2 and Lemma 4.3) in the present setting, with a small extension which can be proven identically. The first lemma resides on the independence of  $(n, M, t_1, \dots, t_n)$  and  $V$  (Assumption 6) together with the classical property of  $L^2$ -optimality of the conditional expectation.

**Lemma 4.1.** *For an  $\mathbb{A}$ -adapted process  $\eta$ , it holds that*

$$\begin{aligned} & \mathbb{E} \left[ \frac{1}{n} \sum_{i=1}^n \left| \text{proj}_V(M_{t_i}) \odot (V_{t_i} - \eta_{t_i-}) \right|_2^2 \right] \\ &= \mathbb{E} \left[ \frac{1}{n} \sum_{i=1}^n \left| \text{proj}_V(M_{t_i}) \odot (V_{t_i} - \hat{V}_{t_i-}) \right|_2^2 \right] + \mathbb{E} \left[ \frac{1}{n} \sum_{i=1}^n \left| \text{proj}_V(M_{t_i}) \odot (\hat{V}_{t_i-} - \eta_{t_i-}) \right|_2^2 \right], \end{aligned}$$

and

$$\begin{aligned} & \mathbb{E} \left[ \frac{1}{n} \sum_{i=1}^n \left| \text{proj}_V(M_{t_i}) \odot (V_{t_i} - \eta_{t_i}) \right|_2^2 \right] \\ &= \mathbb{E} \left[ \frac{1}{n} \sum_{i=1}^n \left| \text{proj}_V(M_{t_i}) \odot (V_{t_i} - \hat{V}_{t_i}) \right|_2^2 \right] + \mathbb{E} \left[ \frac{1}{n} \sum_{i=1}^n \left| \text{proj}_V(M_{t_i}) \odot (\hat{V}_{t_i} - \eta_{t_i}) \right|_2^2 \right]. \end{aligned}$$

Observe that an immediate consequence of this result is that  $\hat{V}$  is  $L^2$  optimal in the sense

$$\mathbb{E} \left[ \frac{1}{n} \sum_{i=1}^n \left| \text{proj}_V(M_{t_i}) \odot (V_{t_i} - \hat{V}_{t_i}) \right|_2^2 \right] = \min_{\eta \in \mathbb{D}} \mathbb{E} \left[ \frac{1}{n} \sum_{i=1}^n \left| \text{proj}_V(M_{t_i}) \odot (V_{t_i} - \eta_{t_i}) \right|_2^2 \right]. \quad (7)$$

The next result derives a highly tractable, linear representation of certain piecewise constant functions of an additional, independent random variable.

**Lemma 4.2.** Consider a stochastic process  $\varphi = (\varphi_t)_{t \in T}$ , bounded from below, an independent random variable  $Y \sim \text{Unif}([0, 1])$  and let  $\bar{t} := \sum_{i=1}^n \mathbf{1}_{(\frac{i-1}{n}, \frac{i}{n}]}(Y) t_i$ . Then,

$$\mathbb{E}[\varphi(\bar{t})] = \mathbb{E}\left[\sum_{i=1}^n \frac{1}{n} \varphi(t_i)\right].$$

Similarly, if  $\bar{t} := \sum_{i=1}^n \mathbf{1}_{(\frac{i-1}{2n}, \frac{i}{2n}]}(Y) t_i + \sum_{i=1}^n \mathbf{1}_{(\frac{n+i-1}{2n}, \frac{n+i}{2n}]}(Y) t_{i-1}$ ,

$$\mathbb{E}[\varphi(\bar{t})] = \frac{1}{2} \left( \mathbb{E}\left[\sum_{i=1}^n \frac{1}{n} \varphi(t_i)\right] + \mathbb{E}\left[\sum_{i=1}^n \frac{1}{n} \varphi(t_{i-1})\right] \right).$$

For intuition, we provide the short proof of this result, following [Krach et al. \(2022\)](#).

*Proof.* Since  $\varphi$  is bounded from below, the expectation is well-defined, although possibly infinite. Furthermore, by independence

$$\begin{aligned} \mathbb{E}[\varphi(\bar{t})] &= \mathbb{E}\left[\int_0^1 \varphi\left(\sum_{i=1}^n \mathbf{1}_{(\frac{i-1}{n}, \frac{i}{n}]}(y) t_i\right) dy\right] \\ &= \int_{\Omega} \int_0^1 \varphi\left(\sum_{i=1}^{n(\omega)} \mathbf{1}_{(\frac{i-1}{n(\omega)}, \frac{i}{n(\omega)}]}(y) t_i(\omega), \omega\right) dy d\mathbb{P} \\ &= \int_{\Omega} \sum_{i=1}^{n(\omega)} \int_{(\frac{i-1}{n(\omega)}, \frac{i}{n(\omega)}]} \varphi(t_i(\omega), \omega) dy d\mathbb{P} = \mathbb{E}\left[\sum_{i=1}^n \frac{1}{n} \varphi(t_i)\right]. \quad \square \end{aligned}$$

Now, we can state the first main convergence result which shows that minima of the theoretical loss function  $L$  defined in Equation (5) converge to the minimal value of  $\Psi$  defined in Equation (4). The result is adapted from [Krach et al. \(2022\)](#). We let  $\Theta_m \subset \Theta$  be the set of combined weights for all 3 neural networks of the IO NJ-ODE that are bounded in 2-norm by  $m$  and correspond to neural networks of width and depth bounded by  $m$ . Overall, the model has the weights  $\theta = (\theta_1, \theta_2, \theta_3) \in \Theta_m$  with  $\theta_i = (\theta_i, \gamma_i)$  for  $i \in \{1, 2\}$ . We denote by  $\Theta_m^i$  and  $\hat{\Theta}_m^i$  the projection of the set  $\Theta_m$  on the weights  $\theta_i$  and  $\hat{\theta}_i$ , respectively.

**Theorem 4.3.** Assume that Assumptions 1 to 5 hold and let  $\theta_m^{\min} \in \Theta_m^{\min} := \text{argmin}_{\theta \in \Theta_m} \{L(\theta)\}$  for every  $m \in \mathbb{N}$ . Then, for  $m \rightarrow \infty$ , the value of minima of the loss function  $L(\theta_m^{\min})$  converge to the minimal value of  $\Psi$ , which is uniquely achieved by  $\hat{V}$  up to indistinguishability on observation points, i.e.,

$$L(\theta_m^{\min}) \xrightarrow{m \rightarrow \infty} \min_{\eta \in \mathbb{D}} \Psi(\eta) = \Psi(\hat{V}).$$

Furthermore, for every  $1 \leq k \leq \bar{n}$ ,  $G_m^{\theta_m^{\min}}$  converges to  $\hat{V}$  in the pseudo metric  $d_k$  as  $m \rightarrow \infty$ .

*Proof. Step 1:* We start by showing that the objective function  $\Psi$  has the unique minimizer  $\hat{V} \in \mathbb{D}$  up to indistinguishability. We first show that  $\hat{V}$  is a minimizer. By Assumption 2,  $\mathbb{P}(\{\Delta V_{t_i} \neq 0 \mid i \leq n\}) = 0$ , such that  $V_{t_{i-}} = V_{t_i}$  with probability one. Then, Lemma 4.1 together with Equation (7) implies that

$$\begin{aligned} \Psi(\hat{V}) &= \mathbb{E}\left[\frac{1}{n} \sum_{i=1}^n \left( \left| \text{proj}_V(M_{t_i}) \odot (V_{t_i} - \hat{V}_{t_i}) \right|_2^2 + \left| \text{proj}_V(M_i) \odot (V_{t_i} - \hat{V}_{t_{i-}}) \right|_2^2 \right)\right] \\ &= \min_{\eta \in \mathbb{D}} \mathbb{E}\left[\frac{1}{n} \sum_{i=1}^n \left( \left| \text{proj}_V(M_i) \odot (V_{t_i} - \eta_{t_i}) \right|_2^2 \right)\right] + \min_{\eta \in \mathbb{D}} \mathbb{E}\left[\frac{1}{n} \sum_{i=1}^n \left( \left| \text{proj}_V(M_i) \odot (V_{t_i} - \eta_{t_{i-}}) \right|_2^2 \right)\right] \\ &\leq \min_{\eta \in \mathbb{D}} \mathbb{E}\left[\frac{1}{n} \sum_{i=1}^n \left( \left| \text{proj}_V(M_i) \odot (V_{t_i} - \eta_{t_i}) \right|_2^2 + \left| \text{proj}_V(M_i) \odot (V_{t_i} - \eta_{t_{i-}}) \right|_2^2 \right)\right] \\ &= \min_{\eta \in \mathbb{D}} \Psi(\eta). \end{aligned}$$



Next, we show uniqueness at observation points. We start by deriving some needed results. Let  $c_1 := \mathbb{E}[n]^{\frac{1}{2}} \in (0, \infty)$ , then we use the Hölder inequality with the fact that  $n \geq 1$  to have

$$\mathbb{E}[|\xi|_2] = \mathbb{E}\left[\frac{\sqrt{n}}{\sqrt{n}}|\xi|_2\right] \leq c_1 \mathbb{E}\left[\frac{1}{n}|\xi|_2^2\right]^{1/2}. \quad (8)$$

According to Assumption 1,  $c_2(k) := \min_{d_U+1 \leq j \leq d} \mathbb{P}(M_{k,j} = 1) > 0$ . Then, we have for any  $1 \leq k \leq \bar{n}$  by the independence of  $\text{proj}_V(M_{k,j})$  from  $t_k$ ,  $n$  and  $\mathcal{A}_{t_k-}$  that

$$\begin{aligned} & \mathbb{E}\left[\mathbf{1}_{\{k \leq n\}} \left( \left| \text{proj}_V(M_{t_k}) \odot (\hat{V}_{t_k-} - \eta_{t_k-}) \right|_1 + \left| \text{proj}_V(M_{t_k}) \odot (\hat{V}_{t_k} - \eta_{t_k}) \right|_1 \right)\right] \\ &= \mathbb{E}\left[\mathbf{1}_{\{k \leq n\}} \sum_{j=d_U+1}^d M_{k,j} \left( \left| \hat{V}_{t_k-,j} - \eta_{t_k-,j} \right| + \left| \hat{V}_{t_k,j} - \eta_{t_k,j} \right| \right)\right] \\ &= \sum_{j=d_U+1}^d \mathbb{E}[M_{k,j}] \mathbb{E}\left[\mathbf{1}_{\{k \leq n\}} \left( \left| \hat{V}_{t_k-,j} - \eta_{t_k-,j} \right| + \left| \hat{V}_{t_k,j} - \eta_{t_k,j} \right| \right)\right] \\ &\geq c_2(k) \mathbb{E}\left[\mathbf{1}_{\{k \leq n\}} \left( \left| \hat{V}_{t_k-} - \eta_{t_k-} \right|_1 + \left| \hat{V}_{t_k} - \eta_{t_k} \right|_1 \right)\right]. \end{aligned}$$

By the equivalence between 1-norm and 2-norm, we have for some constant  $c_3 > 0$

$$\begin{aligned} & \mathbb{E}\left[\mathbf{1}_{\{k \leq n\}} \left( \left| \hat{V}_{t_k-} - \eta_{t_k-} \right|_2 + \left| \hat{V}_{t_k} - \eta_{t_k} \right|_2 \right)\right] \\ &\leq \frac{c_3}{c_2(k)} \mathbb{E}\left[\mathbf{1}_{\{k \leq n\}} \left( \left| \text{proj}_V(M_{t_k}) \odot (\hat{V}_{t_k-} - \eta_{t_k-}) \right|_2 + \left| \text{proj}_V(M_{t_k}) \odot (\hat{V}_{t_k} - \eta_{t_k}) \right|_2 \right)\right]. \end{aligned} \quad (9)$$

To finish the last part of this first step, consider  $\eta \in \mathbb{D}$  which is not indistinguishable from  $\hat{V}$  at observations. Hence, by Definition 2.4, there exists some  $k \in \{1, \dots, \bar{n}\}$  such that  $d_k(\hat{V}, \eta) > 0$ . We have by Lemma 4.1

$$\begin{aligned} \Psi(\eta) &= \mathbb{E}\left[\frac{1}{n} \sum_{i=1}^n \left( \left| \text{proj}_V(M_i) \odot (V_{t_i} - \eta_{t_i}) \right|_2^2 + \left| \text{proj}_V(M_i) \odot (V_{t_i} - \eta_{t_i-}) \right|_2^2 \right)\right] \\ &= \mathbb{E}\left[\frac{1}{n} \sum_{i=1}^n \left| \text{proj}_V(M_{t_i}) \odot (V_{t_i} - \hat{V}_{t_i-}) \right|_2^2\right] + \mathbb{E}\left[\frac{1}{n} \sum_{i=1}^n \left| \text{proj}_V(M_{t_i}) \odot (\hat{V}_{t_i-} - \eta_{t_i-}) \right|_2^2\right] \\ &\quad + \mathbb{E}\left[\frac{1}{n} \sum_{i=1}^n \left| \text{proj}_V(M_{t_i}) \odot (V_{t_i} - \hat{V}_{t_i}) \right|_2^2\right] + \mathbb{E}\left[\frac{1}{n} \sum_{i=1}^n \left| \text{proj}_V(M_{t_i}) \odot (\hat{V}_{t_i} - \eta_{t_i}) \right|_2^2\right] \\ &= \Psi(\hat{V}) + \mathbb{E}\left[\frac{1}{n} \sum_{i=1}^n \left| \text{proj}_V(M_{t_i}) \odot (\hat{V}_{t_i-} - \eta_{t_i-}) \right|_2^2 + \left| \text{proj}_V(M_i) \odot (\hat{V}_{t_i} - \eta_{t_i}) \right|_2^2\right], \end{aligned}$$

and it is now easy to see that the second addend is greater than 0: indeed, we have

$$\begin{aligned} & \mathbb{E}\left[\frac{1}{n} \sum_{i=1}^n \left| \text{proj}_V(M_{t_i}) \odot (\hat{V}_{t_i-} - \eta_{t_i-}) \right|_2^2 + \left| \text{proj}_V(M_i) \odot (\hat{V}_{t_i} - \eta_{t_i}) \right|_2^2\right] \\ &= \mathbb{E}\left[\frac{1}{n} \sum_{i=1}^{\bar{n}} \mathbf{1}_{\{i \leq n\}} \left( \left| \text{proj}_V(M_{t_i}) \odot (\hat{V}_{t_i-} - \eta_{t_i-}) \right|_2^2 + \left| \text{proj}_V(M_i) \odot (\hat{V}_{t_i} - \eta_{t_i}) \right|_2^2 \right)\right] \\ &\geq \mathbb{E}\left[\frac{1}{n} \mathbf{1}_{\{k \leq n\}} \left( \left| \text{proj}_V(M_{t_k}) \odot (\hat{V}_{t_k-} - \eta_{t_k-}) \right|_2^2 + \left| \text{proj}_V(M_{t_k}) \odot (\hat{V}_{t_k} - \eta_{t_k}) \right|_2^2 \right)\right] \\ &\geq \frac{1}{c_1^2} \left( \mathbb{E}\left[\mathbf{1}_{\{k \leq n\}} \left| \text{proj}_V(M_{t_k}) \odot (\hat{V}_{t_k-} - \eta_{t_k-}) \right|_2\right]^2 + \mathbb{E}\left[\mathbf{1}_{\{k \leq n\}} \left| \text{proj}_V(M_{t_k}) \odot (\hat{V}_{t_k} - \eta_{t_k}) \right|_2\right]^2 \right) \end{aligned} \quad (10)$$

using Equation (8) for both addends separately. Moreover,

$$(10) \geq \frac{1}{2c_1^2} \mathbb{E}\left[\mathbf{1}_{\{k \leq n\}} \left( \left| \text{proj}_V(M_{t_k}) \odot (\hat{V}_{t_k-} - \eta_{t_k-}) \right|_2 + \left| \text{proj}_V(M_{t_k}) \odot (\hat{V}_{t_k} - \eta_{t_k}) \right|_2 \right)^2\right]$$

$$\geq \frac{1}{2} \left( \frac{c_2(k)}{c_1 c_3} \right)^2 \mathbb{E} \left[ \mathbf{1}_{\{n \geq k\}} \left( \left| \hat{V}_{t_k^-} - \eta_{t_k^-} \right|_2 + \left| \hat{V}_{t_k} - \eta_{t_k} \right|_2 \right) \right]^2 = \frac{1}{2} \left( \frac{c_2(k)}{c_0(k) c_1 c_3} \right)^2 d_k(\hat{V}, \eta)^2 > 0,$$

where we have used the Cauchy-Schwarz inequality  $(a+b)^2 \leq 2a^2 + 2b^2$ , Equation (9) and finally (2). This gives  $\Psi(\eta) > \Psi(\hat{V})$ , and therefore  $\Psi$  has the unique minimizer  $\hat{V}$ .

**Step 2:** Bounding the distance between  $G^{\theta_m^*}$  and  $\hat{V}$ .

For the second step, we start by showing that the IO NJ-ODE model (3) can approximate  $\hat{V}$  arbitrarily well. Let us fix the dimension  $d_H := d_V$  and choose  $\tilde{\theta}_3^*$  such that  $\tilde{g}_{\theta_3^*} = \text{id}$ . We define for  $\varepsilon > 0$ ,  $N_\varepsilon := \lceil 2(T+1)\varepsilon^{-2} \rceil^2$  and  $\mathcal{P}_\varepsilon$  as the closure of by  $N_\varepsilon$  bounded and piecewise constant functions  $A_{N_\varepsilon}$ , defined in Proposition A.6, which is compact. Using Assumption 3, for any  $j \in [d_U + 1, d]$ , the continuous function  $F_j$  representing  $\hat{V}_j$  can be written as  $F_j(t, \tau(t), \tilde{U}^{\leq \tau(t)} - U_0, U_0)$ . We obtain the approximation  $\hat{F}_j$  which is a function of the truncated signature only by Proposition A.5, i.e., there exist  $m_0 = m_0(\varepsilon) \in \mathbb{N}$  and continuous  $\hat{F}_j$  such that

$$\sup_{(t, \tau, U) \in [0, T]^2 \times \mathcal{P}_\varepsilon} \left| F_j(t, \tau, U) - \hat{F}_j(t, \tau, \pi_{m_0}(U - U_0), U_0) \right| \leq \varepsilon/2.$$

Due to the uniformly bounded variation of functions in  $\mathcal{P}_\varepsilon$ , the set of truncated signatures  $\pi_{m_0}(\mathcal{P}_\varepsilon)$  is bounded in  $\mathbb{R}^{d'}$  for some  $d' \in \mathbb{N}$  (depending on  $d_U$  and  $m_0$ ). Its closure, denoted by  $\Pi_\varepsilon$ , is compact. By the universal approximation theorem for neural networks (Hornik et al., 1989, Theorem 2.4), there exists  $m_{1,1} \in \mathbb{N}$  and neural network weights  $\tilde{\theta}_{1,1}^{*, m_{1,1}} \in \tilde{\Theta}_{m_{1,1}}^1$  such that for each  $j \in [d_U + 1, d]$  the function  $\hat{F}_j$  can be estimated by the  $j$ -th coordinate of the neural network  $\tilde{f}_{\tilde{\theta}_{1,1}^{*, m_{1,1}}}$  on the compact set  $[0, T]^2 \times \Pi_\varepsilon$  within  $\varepsilon/2$ . Thus, we obtain

$$\begin{aligned} & \sup_{(t, \tau, U) \in [0, T]^2 \times \mathcal{P}_\varepsilon} \left| F_j(t, \tau, U) - \tilde{f}_{\tilde{\theta}_{1,1}^{*, m_{1,1}}, j}(t, \tau, \pi_{m_0}(U - U_0), U_0) \right| \\ & \leq \sup_{(t, \tau, U) \in [0, T]^2 \times \mathcal{P}_\varepsilon} \left| F_j(t, \tau, U) - \hat{F}_j(t, \tau, \pi_{m_0}(U - U_0), U_0) \right| \\ & \quad + \sup_{(t, \tau, U) \in [0, T]^2 \times \mathcal{P}_\varepsilon} \left| \hat{F}_j(t, \tau, \pi_{m_0}(U - U_0), U_0) - \tilde{f}_{\tilde{\theta}_{1,1}^{*, m_{1,1}}, j}(t, \tau, \pi_{m_0}(U - U_0), U_0) \right| \leq \varepsilon/2 + \varepsilon/2 = \varepsilon. \end{aligned}$$

Analogously, there exist  $m_{2,1} \in \mathbb{N}$ , neural network weights  $\tilde{\theta}_{2,1}^{*, m_{2,1}} \in \tilde{\Theta}_{m_{2,1}}^2$  and a network  $\tilde{\rho}_{\tilde{\theta}_{2,1}^{*, m_{2,1}}, j} \in \tilde{\mathcal{N}}$  such that for each  $j \in [d_U + 1, d]$

$$\sup_{(t, U) \in [0, T] \times \mathcal{P}_\varepsilon} \left| F_j(t, t, U) - \tilde{\rho}_{\tilde{\theta}_{2,1}^{*, m_{2,1}}, j}(t, \pi_{m_0}(U - U_0), U_0) \right| \leq \varepsilon.$$

We note that we can extend the neural network by adding  $H_{t^-}$  as additional input variable, without decreasing the approximation quality.

Subsequent, we construct the bounded output neural networks by defining  $\gamma_1$  and  $\gamma_2$  as

$$\begin{aligned} \gamma_1 & := \max_{(t, \tau, U) \in [0, T]^2 \times \mathcal{P}_\varepsilon} \left| \tilde{f}_{\tilde{\theta}_{1,1}^{*, m_{1,1}}}(t, \tau, \pi_{m_0}(U - U_0), U_0) \right|. \\ \gamma_2 & := \max_{(t, \tau, U) \in [0, T]^2 \times \mathcal{P}_\varepsilon} \left| \tilde{\rho}_{\tilde{\theta}_{2,1}^{*, m_{2,1}}, j}(t, \pi_{m_0}(U - U_0), U_0) \right|. \end{aligned}$$

Since the maximum of a continuous function on a compact set is finite, both constants are finite. Hence, the bounded output neural networks  $\tilde{f}_{\tilde{\theta}_{1,1}^{*, m_{1,1}}}$ ,  $\tilde{\rho}_{\tilde{\theta}_{2,1}^{*, m_{2,1}}, j} \in \mathcal{N}$  are well defined with  $\tilde{\theta}_{i,1}^{*, m_{i,1}} := (\tilde{\theta}_{i,1}^{*, m_{i,1}}, \gamma_i)$ . As already remarked, the truncation functions coincide with the identity for  $|x|_2 \leq \gamma_i$ ,  $i = 1, 2$ , respectively, and so the bounded networks match the original networks on  $[0, T]^2 \times \mathcal{P}_\varepsilon$  and therefore provide the same  $\varepsilon$ -approximation.

This boundedness alone is insufficient to demonstrate the convergence referred to in this part of the proof. The bounds do not always result in boundedness by  $f_j, F_j$  and depend on  $\varepsilon$ . Specifically, as  $\varepsilon$  decreases

---

<sup>2</sup> $\lceil \cdot \rceil$  is the ceiling function.

and  $m$  increases,  $\gamma_i$  may grow so quickly that the expectation of neural networks outside the compact set does not converge to zero as the compact set expands. Therefore, we compensate these neural networks with additional ones. To ascertain whether the input trajectory resides within the pertinent compact set, we employ the random variables  $\tilde{U}_t^* := \sup_{0 \leq s \leq t} |\tilde{U}_s^{\leq t}|_1 \leq U_T^*$ ,  $n_t := \max\{i \in \mathbb{N} \mid t_i \leq t\} \leq n$  and  $\delta_t := \min\{t_i - t_{i-1} \mid t_i \leq t\} \geq \delta_{\min}$  as supplementary inputs for the neural networks. By assigning the respective weights to zero in the neural networks described previously in **step 2**, the  $\varepsilon$ -approximation remains intact.

On the one hand, if  $\tilde{U}_t^* \leq 1/\varepsilon$ ,  $n_t \leq 1/\varepsilon$ , and  $\delta_t \geq \varepsilon$ , then  $\tilde{U}^{\leq t} - U_0 \in A_{N_\varepsilon} \subset \mathcal{P}_\varepsilon$ , thereby ensuring the  $\varepsilon$ -approximation holds. On the other hand, we have to study the case where either  $U_T^* > 1/\varepsilon$ ,  $n > 1/\varepsilon$ , or  $\delta_{\min} < \varepsilon$ . We define  $\tilde{\mu}_1$  to be the push-forward measure of  $dt \times \mathbb{P}$  through the measurable map  $\tilde{\mu}_1 : [0, T] \times \Omega \rightarrow \mathbb{R}^{2+d'+d_V+3}$  given by

$$\tilde{\mu}_1(t) = (t, \tau(t), \pi_{m_0}(\tilde{U}^{\leq t} - U_0), U_0, U_t^*, n_t, \delta_t). \quad (11)$$

Moreover, we define  $D_1 := [0, T]^2 \times \mathbb{R}^{d'} \times \mathbb{R}^{d_V} \times [0, 1/\varepsilon]^2 \times [\varepsilon, T]$ . We denote the complement as  $D_1^c$ , and define

$$v := \bar{f}_{\theta_{1,1}^*, m_{1,1}} \mathbf{1}_{D_1^c} : \mathbb{R}^{2+d'+d_V} \rightarrow \mathbb{R}^{d_V}.$$

Thus,  $\tilde{\mu}_1(\mathbb{R}^{2+d'+d_V+3}) = T$ , which means that  $\tilde{\mu}_1$  is a finite measure. Furthermore,  $v$  belongs to  $L^2(\tilde{\mu}_1)$  as it is bounded by  $\gamma_1$ . So, According to [Hornik \(1991, Theorem 1\)](#), there exists  $m_{1,2} \in \mathbb{N}$  and neural network weights  $\tilde{\theta}_{1,2}^{*, m_{1,2}} \in \tilde{\Theta}_{m_{1,2}}^1$  such that the corresponding neural network  $\tilde{f}_{\tilde{\theta}_{1,2}^{*, m_{1,2}}}$  satisfies  $\int |v - \tilde{f}_{\tilde{\theta}_{1,2}^{*, m_{1,2}}}|_2^2 d\tilde{\mu}_1 < \varepsilon$ .

We can assume  $\tilde{f}_{\tilde{\theta}_{1,2}^{*, m_{1,2}}} \in \mathcal{N}$ , which means that this is an output-bounded neural network. Then we define the first new neural network  $f_{\theta_1^*, m_1} = \bar{f}_{\theta_{1,1}^*, m_{1,1}} - \tilde{f}_{\tilde{\theta}_{1,2}^{*, m_{1,2}}} \in \mathcal{N}$ , with the weights  $\theta_1^{*, m_1} = (\bar{\theta}_{1,1}^{*, m_{1,1}}, \tilde{\theta}_{1,2}^{*, m_{1,2}})$  and  $m_1 = m_{1,1} + m_{1,2}$ .

We follow an analogous approach for  $F_j$ , noting that the process varies slightly due to the differences in the push-forward map. We define  $\tilde{\mu}_2$  to be the push-forward measure of  $dq \times \mathbb{P}$  (where  $dq$  denotes the Lebesgue measure) through the measurable map  $\tilde{\mu}_2 : [0, 1] \times \Omega \rightarrow \mathbb{R}^{1+d'+d_V+3}$  defined by

$$\mu(Q, \omega) = (\bar{t}, \pi_{m_0}(\tilde{U}^{\leq \bar{t}} - U_0), U_0, U_{\bar{t}}^*, n_{\bar{t}}, \delta_{\bar{t}}), \quad (12)$$

where  $\bar{t} := \bar{t}(Q, (\omega, \tilde{\omega})) := \sum_{i=1}^n \mathbf{1}_{(\frac{i-1}{2^n}, \frac{i}{2^n}]}(Q) t_i(\tilde{\omega}) + \sum_{i=1}^n \mathbf{1}_{(\frac{n+i-1}{2^n}, \frac{n+i}{2^n}]}(Q) t_{i-1}(\tilde{\omega})$  as in [Lemma 4.2](#). Let  $D_2 := [0, T]^2 \times \mathbb{R}^{d'} \times \mathbb{R}^{d_V} \times [0, 1/\varepsilon]^2 \times [\varepsilon, T]$  and also define

$$\Upsilon := \bar{\rho}_{\theta_{2,1}^*, m_{2,1}} \mathbf{1}_{D_2^c} : \mathbb{R}^{2+d'+d_V} \rightarrow \mathbb{R}^{d_V}.$$

Then,  $\tilde{\mu}_2(\mathbb{R}^{1+d'+d_V+3}) = 1$ , i.e.,  $\tilde{\mu}_2$  is a finite measure and  $\Upsilon$  is a function in  $L^2(\tilde{\mu}_2)$ , since it is bounded by  $\gamma_2$ . According to [Hornik \(1991, Theorem 1\)](#), there exists  $m_{2,2} \in \mathbb{N}$  and neural network weights  $\tilde{\theta}_{2,2}^{*, m_{2,2}} \in \tilde{\Theta}_{m_{2,2}}^2$  such that the corresponding neural network  $\tilde{\rho}_{\tilde{\theta}_{2,2}^{*, m_{2,2}}}$  satisfies  $\int |\Upsilon - \tilde{\rho}_{\tilde{\theta}_{2,2}^{*, m_{2,2}}}|_2^2 d\tilde{\mu}_2 < \varepsilon$ . Then we define the (new) neural network  $\rho_{\theta_2^*, m_2} = \bar{\rho}_{\bar{\theta}_{2,1}^*, m_{2,1}} - \tilde{\rho}_{\tilde{\theta}_{2,2}^{*, m_{2,2}}} \in \mathcal{N}$ , with the weights  $\theta_2^{*, m_2} = (\bar{\theta}_{2,1}^{*, m_{2,1}}, \tilde{\theta}_{2,2}^{*, m_{2,2}})$  and  $m_2 = m_{2,1} + m_{2,2}$ . It is important to recognize that we can't directly approximate  $f$ ,  $F$  or the difference between them and their initial approximating neural networks because the input space of  $f$  and  $F$  is infinite-dimensional. This scenario is not addressed by universal approximation theorems.

Setting  $m := \max(m_0, m_1, m_2, \gamma_1, \gamma_2, |\tilde{\theta}_1^{*, m_1}|_2, |\tilde{\theta}_2^{*, m_2}|_2)$ , it follows that  $\theta_m^* := (\theta_1^{*, m_1}, \theta_2^{*, m_2}, \tilde{\theta}_3^*) \in \Theta_m$ .

We can then finalize the purpose of this **step 2**. Throughout the rest of the proof, we will use the notation

$$\zeta := \left( \mathbf{1}_{\{U_T^* \geq 1/\varepsilon\}} + \mathbf{1}_{\{n \geq 1/\varepsilon\}} + \mathbf{1}_{\{\delta \leq \varepsilon\}} \right), \quad (13)$$

and we know by the argument above that on  $D_i$  the  $\varepsilon$ -approximation holds for any input of the form [\(11\)](#) or [\(12\)](#) respectively, while we have  $\mathbf{1}_{D_i^c} \leq \zeta$  for  $i = 1, 2$  and any potential input where the  $t$  coordinates are

within  $[0, T]$ . we set  $F = (F_j)_{d_U+1 \leq j \leq d}$  and  $f = (f_j)_{d_U+1 \leq j \leq d}$ . For  $t \in \{t_1, \dots, t_n\} \subset [0, T]$  we have with  $\mathbf{1}_{D_2} + \mathbf{1}_{D_2^c} = 1$  and by triangle inequality that

$$\begin{aligned}
\left| G_t^{\theta^*} - \hat{V}_t \right|_1 &= \left| \rho_{\theta_2^*, m_2} (H_{t-}, t, \pi_m(\tilde{U}^{\leq t} - U_0), U_0, U_t^*, n_t, \delta_t) - F(t, t, \tilde{U}^{\leq t}) \right|_1 \\
&= \left| \rho_{\theta_2^*, m_2} - F \right|_1 (\mathbf{1}_{D_2} + \mathbf{1}_{D_2^c}), \\
&\leq \left( \left| \bar{\rho}_{\theta_2^*, m_2, 1} - F \right|_1 + \left| \bar{\rho}_{\theta_2^*, m_2, 2} \right|_1 \right) \mathbf{1}_{D_2} + \left( \left| \bar{\rho}_{\theta_2^*, m_2, 1} - \bar{\rho}_{\theta_2^*, m_2, 2} \right|_1 + |F|_1 \right) \mathbf{1}_{D_2^c} \\
&\leq \left( \epsilon d + \left| \Upsilon - \bar{\rho}_{\theta_2^*, m_2, 2} \right|_1 \right) \mathbf{1}_{D_2} + \left( \left| \Upsilon - \bar{\rho}_{\theta_2^*, m_2, 2} \right|_1 + |F|_1 \right) \mathbf{1}_{D_2^c} \\
&\leq \epsilon d + \left| \left( \Upsilon - \bar{\rho}_{\theta_2^*, m_2, 2} \right) (t) \right|_1 + |F(t)|_1 \zeta,
\end{aligned}$$

where we write  $(t)$  to specify the time input for the respective functions (e.g.,  $F(t)$ ). For  $t \in [0, T] \setminus \{t_1, \dots, t_n\}$ ,

$$\begin{aligned}
\left| G_t^{\theta^*} - \hat{V}_t \right|_1 &\leq \left| G_{\tau(t)}^{\theta^*} - \hat{V}_{\tau(t)} \right|_1 \\
&\quad + \int_{\tau(t)}^t \left| f_{\theta_1^*, m_1} (H_{s-}, s, \tau(t), \pi_m(\tilde{U}^{\leq \tau(t)} - U_0), U_0, U_t^*, n_t, \delta_t) - f(s, \tau(t), \tilde{U}^{\leq \tau(t)}) \right|_1 ds \\
&\leq \left( \epsilon d + \left| \left( \Upsilon - \bar{\rho}_{\theta_2^*, m_2, 2} \right) (\tau(t)) \right|_1 + |F(\tau(t))|_1 \zeta \right) + \int_0^T \left( \epsilon d + \left| v - \tilde{f}_{\theta_1^*, m_1, 2} \right|_1 + |f|_1 \zeta \right) ds,
\end{aligned}$$

Using the same arguments for norm equivalence as in **step 1**, there exists a constant  $c > 0$  such that for all  $t \in [0, T]$

$$\left| G_t^{\theta^*} - \hat{V}_t \right|_2 \leq c \left( \epsilon(1+T)d + \left| \left( \Upsilon - \bar{\rho}_{\theta_2^*, m_2, 2} \right) \right|_2 + \left( |F|_2 + \int_0^T |f(t)|_2 dt \right) \zeta + \int_0^T \left| v - \tilde{f}_{\theta_1^*, m_1, 2} \right|_2 ds \right).$$

We have the bound

$$\begin{aligned}
&\mathbb{E} \left[ \frac{1}{n} \sum_{i=1}^n \left| G_{t_i}^{\theta^*} - \hat{V}_{t_i} \right|_2^2 \right] + \mathbb{E} \left[ \frac{1}{n} \sum_{i=1}^n \left| G_{t_i}^{\theta^*} - \hat{V}_{t_i} \right|_2^2 \right] \\
&\leq 7 \left( \epsilon^2((1+T)d)^2 + \mathbb{E} \left[ \left( \frac{1}{n} \sum_{i=1}^n \left( |F(t_i)|_2^2 + |F(t_{i-1})|_2^2 \right) + \left( \int_0^T |f(t)|_2 dt \right)^2 \right) \zeta \right] \right. \\
&\quad + \mathbb{E} \left[ \frac{1}{n} \sum_{i=1}^n \left| \left( \Upsilon - \bar{\rho}_{\theta_2^*, m_2, 2} \right) (t_{i-1}) \right|_2^2 \right] \\
&\quad \left. + \mathbb{E} \left[ \frac{1}{n} \sum_{i=1}^n \left| \left( \Upsilon - \bar{\rho}_{\theta_2^*, m_2, 2} \right) (t_i) \right|_2^2 \right] + \mathbb{E} \left[ \left( \int_0^T \left| v - \tilde{f}_{\theta_1^*, m_1, 2} \right|_2 ds \right)^2 \right] \right) \\
&\leq 7 \left( \epsilon^2((1+T)d)^2 + \mathbb{E}_{\mu_Q \times \mathbb{P}} \left[ |F(\bar{t})|_2^2 \zeta \right] + \mathbb{E} \left[ T \int_0^T |f(t)|_2^2 dt \zeta \right] \right. \\
&\quad \left. + \mathbb{E}_{\mu_Q \times \mathbb{P}} \left[ \left| \left( \Upsilon - \bar{\rho}_{\theta_2^*, m_2, 2} \right) (\bar{t}) \right|_2^2 \right] + \mathbb{E} \left[ T \int_0^T \left| v - \tilde{f}_{\theta_1^*, m_1, 2} \right|_2^2 ds \right] \right) \tag{14} \\
&= 7 \left( \epsilon^2((1+T)d)^2 + \mathbb{E}_{\mu_Q \times \mathbb{P}} \left[ |F(\bar{t})|_2^2 \zeta \right] + \mathbb{E} \left[ T \int_0^T |f(t)|_2^2 dt \zeta \right] \right. \\
&\quad \left. + \int \left| \Upsilon - \bar{\rho}_{\theta_2^*, m_2, 2} \right|_2^2 d\tilde{\mu}_2 + T \int \left| v - \tilde{f}_{\theta_1^*, m_1, 2} \right|_2^2 d\tilde{\mu}_1 \right) \\
&= 7 \left( \epsilon^2((1+T)d)^2 + \mathbb{E}_{\mu_Q \times \mathbb{P}} \left[ |F(\bar{t})|_2^2 \zeta \right] + \mathbb{E} \left[ T \int_0^T |f(t)|_2^2 dt \zeta \right] + \epsilon(1+T) \right),
\end{aligned}$$

where we used Cauchy-Schwarz inequality in the first inequality. For the second inequality, we used Lemma 4.2 for the second, third and fourth term and for second and the last term, we used Hölder inequality for  $p = q = 2$ . For the third equality we used the definition of the push-forward measures  $\tilde{\mu}_1, \tilde{\mu}_2$  and we applied the  $L^2$  approximation for  $\nu$  and  $\Upsilon$  through the designated neural networks for the last one.

Now, we want to show the  $\varepsilon$ -error converges to 0 when increasing the truncation level and network size  $m \in \mathbb{N}$ . To do that, we define  $\varepsilon_m \geq 0$  to be the smallest number such that the bounds given above with error  $\varepsilon_m$  when using an architecture with signature truncation level  $m$  and weights in  $\Theta_m$ . Increasing  $m$  can only improve the approximation, and we have proven before that for any  $\varepsilon$  there exists some  $m$  such that the  $\varepsilon$ -approximation holds. Hence,  $\lim_{m \rightarrow \infty} \varepsilon_m = 0$ . Let  $\theta_m^* \in \Theta_m$  denote the choice for the neural networks' weights as described above. By hypothesis,  $\theta_m^{\min} \in \operatorname{argmin}_{\theta \in \Theta_m} \{L(\theta)\}$ , therefore, we obtain for  $\bar{t} := \sum_{i=1}^n \mathbf{1}_{(\frac{i-1}{n}, \frac{i}{n}]}(Q) t_i$  with  $Q \sim \operatorname{Unif}([0, 1])$  independent of  $\mathcal{F}$  and  $R_{t_i}^2 := \left| G_{t_i-}^{\theta_m^*} - \hat{V}_{t_i-} \right|_2^2 + \left| G_{t_i}^{\theta_m^*} - \hat{V}_{t_i} \right|_2^2$

$$\begin{aligned}
\min_{\eta \in \mathbb{D}} \Psi(\eta) &\leq L(\theta_m^{\min}) \leq L(\theta_m^*) \\
&= \mathbb{E} \left[ \frac{1}{n} \sum_{i=1}^n \left( \left| \operatorname{proj}_V(M_{t_i}) \odot (V_{t_i} - G_{t_i}^{\theta_m^*}) \right|_2^2 + \left| \operatorname{proj}_V(M_{t_i}) \odot (V_{t_i} - G_{t_i-}^{\theta_m^*}) \right|_2^2 \right) \right] \\
&= \mathbb{E} \left[ \frac{1}{n} \sum_{i=1}^n \left( \left| \operatorname{proj}_V(M_{t_i}) \odot (V_{t_i} - \hat{V}_{t_i}) \right|_2^2 + \left| \operatorname{proj}_V(M_{t_i}) \odot (\hat{V}_{t_i} - G_{t_i}^{\theta_m^*}) \right|_2^2 \right. \right. \\
&\quad \left. \left. + \left| \operatorname{proj}_V(M_{t_i}) \odot (V_{t_i} - \hat{V}_{t_i-}) \right|_2^2 + \left| \operatorname{proj}_V(M_{t_i}) \odot (\hat{V}_{t_i-} - G_{t_i-}^{\theta_m^*}) \right|_2^2 \right) \right] \\
&\leq \Psi(\hat{V}) + \mathbb{E} \left[ \frac{1}{n} \sum_{i=1}^n R_{t_i}^2 \right], \tag{15}
\end{aligned}$$

whereby the 4th (in)equality follows from Lemma 4.1. Together with Assumption 2.1 on  $\delta_{\min}$ , integrability of  $|U_T^*|_2$  and  $|n|$  (Assumptions 4 and 5) suggest that

$$\zeta := \mathbf{1}_{\{U_T^* \geq 1/\varepsilon_m\}} + \mathbf{1}_{\{n \geq 1/\varepsilon_m\}} + \mathbf{1}_{\{\delta \leq \varepsilon_m\}} \xrightarrow[m \rightarrow \infty]{\mathbb{P}\text{-a.s.}} 0.$$

Using this and (14) together with Assumption 3, we get by dominated convergence that

$$\mathbb{E} \left[ \frac{1}{n} \sum_{i=1}^n R_{t_i}^2 \right] \xrightarrow{m \rightarrow \infty} 0.$$

With this limit and the fact that  $\Psi(\hat{V}) = \min_{\eta \in \mathbb{D}} \Psi(\eta)$ , we directly obtain from (15)

$$\min_{\eta \in \mathbb{D}} \Psi(\eta) \leq L(\theta_m^{\min}) \leq L(\theta_m^*) \xrightarrow{m \rightarrow \infty} \min_{\eta \in \mathbb{D}} \Psi(\eta).$$

**Step 3:** For every  $1 \leq k \leq K$  we want to show that  $G^{\theta_m^{\min}}$  converges to  $\hat{V}$  in the metric  $d_k$  as  $m \rightarrow \infty$  i.e.  $\lim_{m \rightarrow \infty} d_k(\hat{V}, G^{\theta_m^{\min}}) = 0$  for all  $1 \leq k \leq K$ . First, Lemma 4.1 yields

$$\begin{aligned}
L(\theta_m^{\min}) - \Psi(\hat{V}) &= \mathbb{E} \left[ \frac{1}{n} \sum_{i=1}^n \left| \operatorname{proj}_V(M_{t_i}) \odot (\hat{V}_{t_i-} - G_{t_i-}^{\theta_m^{\min}}) \right|_2^2 \right] \\
&\quad + \mathbb{E} \left[ \frac{1}{n} \sum_{i=1}^n \left| \operatorname{proj}_V(M_i) \odot (\hat{V}_{t_i} - G_{t_i}^{\theta_m^{\min}}) \right|_2^2 \right]. \tag{16}
\end{aligned}$$

Hence, applying (8), (9) and finally (16), yields

$$d_k(\hat{V}, G^{\theta_m^{\min}}) \leq \frac{c_0(k) c_1 c_3}{c_2(k)} \left( L(\theta_m^{\min}) - \Psi(\hat{V}) \right)^{1/2} \xrightarrow{m \rightarrow \infty} 0, \tag{17}$$

completing the proof.  $\square$

## 4.2 Convergence of the Monte Carlo Approximation

In this section, we present the convergence with respect to the Monte Carlo approximation  $\hat{L}_N$  as the number of samples  $N$  increases. This result builds on and extends [Krach et al. \(2022, Theorem 4.4\)](#). Throughout this section, we assume that the size  $m$  of the neural network and the signature truncation level are fixed.

**Theorem 4.4.** *Let  $\theta_{m,N}^{\min} \in \Theta_{m,N}^{\min} := \operatorname{argmin}_{\theta \in \Theta_m} \{\hat{L}_N(\theta)\}$  for all  $m, N \in \mathbb{N}$ . Then, for each  $m \in \mathbb{N}$ , we have  $(\mathbb{P} \times \tilde{\mathbb{P}})$ -almost surely as  $N \rightarrow \infty$  that*

- $\hat{L}_N$  converges uniformly to  $L$  on  $\Theta_m$ ,
- $L(\theta_{m,N}^{\min})$  converges to  $L(\theta_m^{\min})$  and
- $\hat{L}_N(\theta_{m,N}^{\min})$  converges to  $L(\theta_m^{\min})$ .

Furthermore, there exists an increasing random sequence  $(N_m)_{m \in \mathbb{N}}$  in  $\mathbb{N}$  such that for every  $1 \leq k \leq K$ , it holds almost surely that  $\lim_{m \rightarrow \infty} d_k(\hat{V}, G^{\theta_{m,N_m}^{\min}}) = 0$ .

Before giving the proof, we introduce some additional notation and helpful results. We define the separable Banach space  $\mathcal{S} := \{x = (x_i)_{i \in \mathbb{N}} \in \ell^1(\mathbb{R}^{d_s}) \mid \|x\|_{\ell^1} < \infty\}$  for an appropriate  $d_s \in \mathbb{N}$ , equipped with the norm  $\|x\|_{\ell^1} := \sum_{i \in \mathbb{N}} |x_i|_2$ . Moreover, we define the function

$$\phi(x, y, z, p) := |p \odot (x - y)|_2^2 + |p \odot (x - z)|_2^2$$

and  $\xi_j := (\xi_{j,0}, \dots, \xi_{j,n^{(j)}}), 0, \dots)$ , where  $\xi_{j,k} := (t_k^{(j)}, U_{t_k^{(j)}}^{(j)}, M_{t_k^{(j)}}^{(j)}, \pi_m(\tilde{U}^{\leq t_k^{(j)},(j)} - U_0^{(j)}), \tilde{U}_t^{*,(j)}, k, \delta_{t_k^{(j)}}^{(j)}) \in \mathbb{R}^{d_s}$ .

Let  $n^j(\xi_j) := \max_{k \in \mathbb{N}} \{\xi_{j,k} \neq 0\}$ ,  $t_k(\xi_j) := t_k^{(j)}$ ,  $V_k(\xi_j) := V_{t_k^{(j)}}^{(j)}$  and  $M_k(\xi_j) := M_{t_k^{(j)}}^{(j)}$ . Then we have  $n^{(j)} = n^j(\xi_j)$   $\mathbb{P}$ -almost-surely. Additionally, we know that  $\xi_j$  are i.i.d. random variables taking values in  $\mathcal{S}$ . As before, we write  $G^\theta$  to emphasize the dependence of the model output on the network weights  $\theta$  and define

$$W(\theta, \xi_j) := \frac{1}{n^j(\xi_j)} \sum_{i=1}^{n^j(\xi_j)} \phi\left(V_i(\xi_j), G_{t_i(\xi_j)}^\theta(\xi_j), G_{t_i(\xi_j)-}^\theta(\xi_j), \operatorname{proj}_V(M_i(\xi_j))\right).$$

The following results were proven in [Krach et al. \(2022\)](#).

**Lemma 4.5.** *For every  $t \in [0, T]$ , the random function  $\theta \in \Theta_M \mapsto G_t^\theta$  is uniformly continuous almost surely.*

**Lemma 4.6.** *Let  $(\xi_i)_{i \geq 1}$  be a sequence of i.i.d. random variables with values in  $\mathcal{S}$  and  $W : \mathbb{R}^m \times \mathcal{S} \rightarrow \mathbb{R}$  be a measurable function. Assume that a.s., the function  $\theta \in \mathbb{R}^m \mapsto W(\theta, \xi_1)$  is continuous and for all  $C > 0$ ,  $\mathbb{E}(\sup_{|\theta|_2 \leq C} |W(\theta, \xi_1)|) < +\infty$ . Then, a.s.  $f_N : \mathbb{R}^m \rightarrow \mathbb{R}, \theta \mapsto \frac{1}{N} \sum_{i=1}^N W(\theta, \xi_i)$  converges locally uniformly to the continuous function  $f : \mathbb{R}^m \rightarrow \mathbb{R}, \theta \mapsto \mathbb{E}(W(\theta, \xi_1))$ , i.e.,*

$$\lim_{N \rightarrow \infty} \sup_{|\theta|_2 \leq C} \left| \frac{1}{N} \sum_{i=1}^N W(\theta, \xi_i) - \mathbb{E}(W(\theta, \xi_1)) \right| = 0 \quad \text{a.s.}$$

Additionally, let  $K \subset \mathbb{R}^m$  be compact and define the random variables  $v_n := \inf_{x \in K} f_n(x)$ . We consider a minimizing sequence of random variables  $(x_n)_{n=0}^\infty$ , given by  $f_n(x_n) = \inf_{x \in K} f_n(x)$  and let  $v^* = \inf_{x \in K} f(x)$  and  $\mathcal{K}^* = \{x \in K : f(x) = v^*\}$ . Then  $v_n \rightarrow v^*$  and  $\min_{z \in \mathcal{K}^*} |x_n - z|_2 \rightarrow 0$  a.s. as  $n \rightarrow \infty$ .

We can now proceed with the proof of [Theorem 4.4](#).

*Proof of [Theorem 4.4](#). Step 1:* we show that  $\hat{L}_N(\theta) \xrightarrow{N \rightarrow \infty} L(\theta)$  uniformly on  $\Theta_m$ .

Fix  $m \in \mathbb{N}$ . Since  $G_t^\theta$  is the output of neural networks with bounded outputs, it is bounded in terms of the input, the weights (bounded by  $m$ ), the time interval  $T$ , and certain constants depending on the network's architecture and activation functions. Specifically, for all  $t \in [0, T]$  and  $\theta \in \Theta_m$ , we have

$|G_t^\theta(\xi_j)| \leq \tilde{B}(1 + U^{*,(j)})$ , where  $U^{*,(j)}$  corresponds to the input  $\xi_j$  and  $\tilde{B}$  is a constant that may depend on  $m$ . Therefore, we have

$$\begin{aligned} & \phi \left( V_i(\xi_j), G_{t_i(\xi_j)}^\theta(\xi_j), G_{t_i(\xi_j)-}^\theta(\xi_j), \text{proj}_V(M_i(\xi_j)) \right) \\ &= \left| \text{proj}_V(M_i(\xi_j)) \odot (V_i(\xi_j) - G_{t_i(\xi_j)}^\theta(\xi_j)) \right|_2^2 + \left| \text{proj}_V(M_i(\xi_j)) \odot (V_i(\xi_j) - G_{t_i(\xi_j)-}^\theta(\xi_j)) \right|_2^2 \\ &\leq 4 \left( \tilde{B}^2(1 + U^{*,(j)})^2 + (V_{t_i}^{(j)})^2 \right). \end{aligned}$$

Using the integrability of  $U$  and  $V$  describe in Assumption 4 we have

$$\mathbb{E} \left[ \sup_{\theta \in \Theta_m} |W(\theta, \xi_j)| \right] \leq \mathbb{E} \left[ \frac{1}{n^j(\xi_j)} \sum_{i=1}^{n^j(\xi_j)} 4 \left( \tilde{B}^2(1 + U^{*,(j)})^2 + (V_{t_i}^{(j)})^2 \right) \right] < \infty. \quad (18)$$

Using Lemma 4.5, the function  $\theta \mapsto W(\theta, \xi_1)$  is continuous, therefore, Lemma 4.6 implies that a.s for  $N \rightarrow \infty$ , the function

$$\theta \mapsto \frac{1}{N} \sum_{i=1}^N W(\theta, \xi_i) = \hat{L}_N(\theta) \quad (19)$$

converges locally uniformly on  $\Theta_m$  to the continuous function

$$\theta \mapsto \mathbb{E}[W(\theta, \xi_1)] = L(\theta). \quad (20)$$

**Step 2:** we show that  $L(\theta_{m,N}^{\min}) \xrightarrow{N \rightarrow \infty} L(\theta_m^{\min})$  and  $\hat{L}_N(\theta_{m,N}^{\min}) \xrightarrow{N \rightarrow \infty} L(\theta_m^{\min})$ .

Lemma 4.6 also implies that  $\lim_{N \rightarrow \infty} \min_{\vartheta \in \Theta_m^{\min}} |\theta_{m,N}^{\min} - \vartheta|_2 = 0$  (a.s.). Thus there exists a sequence  $(\hat{\theta}_{m,N}^{\min})_{N \in \mathbb{N}}$  in  $\Theta_m^{\min}$  such that  $\lim_{N \rightarrow \infty} |\theta_{m,N}^{\min} - \hat{\theta}_{m,N}^{\min}|_2 = 0$  (a.s.). Since the function  $\theta \mapsto G_t^\theta$  on  $\Theta_m$  is uniformly continuous, we have for any fixed deterministic and bounded  $\xi_0$

$$\lim_{N \rightarrow \infty} |G_t^{\theta_{m,N}^{\min}}(\xi_0) - G_t^{\hat{\theta}_{m,N}^{\min}}(\xi_0)|_2 = 0 \text{ a.s. for all } t \in [0, T].$$

Using the fact that  $\phi$  is continuous, we get  $\lim_{N \rightarrow \infty} |W(\theta_{m,N}^{\min}, \xi_0) - W(\hat{\theta}_{m,N}^{\min}, \xi_0)| = 0$  (a.s.). We assume now that  $\xi_0$  is an i.i.d. random variable distributed as the  $\xi_j$  defined on a copy  $(\Omega_0, \mathbb{F}_0, \mathcal{F}_0, \mathbb{P}_0)$  of the filtered probability space  $(\Omega, \mathbb{F}, \mathcal{F}, \mathbb{P})$ . Then for  $\mathbb{P}_0$ -almost every fixed  $w_0$ , we have

$$\lim_{N \rightarrow \infty} |W(\theta_{m,N}^{\min}, \xi_0(w_0)) - W(\hat{\theta}_{m,N}^{\min}, \xi_0(w_0))| = 0 \quad (\text{a.s.}).$$

Hence we have for  $\mathbb{P}$ -a.e. fixed  $\omega \in \Omega$ , that  $|W(\theta_{m,N}^{\min}(\omega), \xi_0) - W(\hat{\theta}_{m,N}^{\min}(\omega), \xi_0)| \rightarrow 0$   $\mathbb{P}_0$ -a.s. as  $N \rightarrow \infty$ . Using (18), we apply the dominated convergence theorem, leading to

$$\lim_{N \rightarrow \infty} \mathbb{E}_{\xi_0} \left[ |W(\theta_{m,N}^{\min}(\omega), \xi_0) - W(\hat{\theta}_{m,N}^{\min}(\omega), \xi_0)| \right] = 0,$$

for  $\mathbb{P}$ -a.e.  $\omega \in \Omega$ . We note that  $\omega$  corresponds to the realisation of the training samples, which lead to the trained parameters, while  $\omega_0$  and  $\xi_0$  correspond to the validation or test samples (which can also coincide with the training samples, see below). We know that for every integrable random variable  $Z$ , we have  $0 \leq |\mathbb{E}[Z]| \leq \mathbb{E}[|Z|]$  and noting that  $\hat{\theta}_{m,N}^{\min} \in \Theta_m^{\min}$  we can deduce that for  $\mathbb{P}$ -almost every fixed  $\omega \in \Omega$ ,

$$\lim_{N \rightarrow \infty} L(\theta_{m,N}^{\min}(\omega)) = \lim_{N \rightarrow \infty} \mathbb{E}_{\xi_0} [W(\theta_{m,N}^{\min}(\omega), \xi_0)] = \lim_{N \rightarrow \infty} \mathbb{E}_{\xi_0} [W(\hat{\theta}_{m,N}^{\min}(\omega), \xi_0)] = L(\theta_m^{\min}). \quad (21)$$

For  $\mathbb{P}$ -a.e. fixed  $\omega$ , we have for  $\hat{L}_{\tilde{N}}$  and  $L$  defined through test samples  $\tilde{\xi}_j$  on  $\Omega_0$  that

$$|\hat{L}_{\tilde{N}}(\theta_{m,N}^{\min}(\omega)) - L(\theta_m^{\min})| \leq |\hat{L}_{\tilde{N}}(\theta_{m,N}^{\min}(\omega)) - L(\theta_{m,N}^{\min}(\omega))| + |L(\theta_{m,N}^{\min}(\omega)) - L(\theta_m^{\min})|. \quad (22)$$

Using **step 1** when  $\tilde{N} \rightarrow \infty$ , the first term on the right side goes to 0 and with (21), the second term goes to 0. Now, due to the uniform convergence in (19) and (20), we have the same convergence when setting  $\tilde{N} = N$ , i.e., when evaluating on the training samples. Therefore, we have shown that  $L(\theta_{m,N}^{\min}) \xrightarrow{N \rightarrow \infty} L(\theta_m^{\min})$  and  $\hat{L}_N(\theta_{m,N}^{\min}) \xrightarrow{N \rightarrow \infty} L(\theta_m^{\min})$ .

**Step 3:** Finally, we show convergence in  $d_k$ .

Define  $N_0 := 0$  and for each  $m \in \mathbb{N}$ ,

$$N_m(\omega) := \min \left\{ N \in \mathbb{N} \mid N > N_{m-1}(\omega), |L(\theta_{m,N}^{\min}(\omega)) - L(\theta_m^{\min})| \leq \frac{1}{m} \right\},$$

which is achievable due to (21) for almost every  $\omega \in \Omega$  under  $(\mathbb{P} \times \tilde{\mathbb{P}})$ . With Theorem 4.3, this choice of  $N_m$  implies that for almost every  $\omega \in \Omega$ ,

$$\left| L(\theta_{m,N_m(\omega)}^{\min}(\omega)) - \Psi(\hat{V}) \right| \leq \frac{1}{m} + \left| L(\theta_m^{\min}) - \Psi(\hat{V}) \right| \xrightarrow{m \rightarrow \infty} 0.$$

Thus, by employing similar arguments as in the proof of Theorem 4.3 (starting from (16)), we can demonstrate that

$$d_k \left( \hat{V}, G^{\theta_{m,N_m(\omega)}^{\min}(\omega)} \right) \leq \frac{c_0(k) c_1 c_3}{c_2} \left( L(\theta_{m,N_m(\omega)}^{\min}(\omega)) - \Psi(\hat{V}) \right)^{1/2} \xrightarrow{m \rightarrow \infty} 0,$$

for each  $1 \leq k \leq K$  and for almost every  $\omega \in \Omega$  under  $(\mathbb{P} \times \tilde{\mathbb{P}})$ .  $\square$

### 4.3 Different Observation Times for Input and Output Variables

Our model can also deal with settings, where inputs and outputs are not observed simultaneously. In our notation, this means that certain input or output coordinates are masked via the observation mask  $M$ .

In some real-world applications, there is zero probability of observing the input and the output at exactly the same time. Then Assumption 1 would be violated. However, the following corollary shows how this assumption can be relaxed.

**Corollary 4.7.** *When we remove the condition,*

$$\mathbb{P}(M_{k,j} = 1) > 0 \text{ for all } d_U + 1 \leq j \leq d \tag{23}$$

*of Assumption 1 we still obtain all the results of Theorem 4.3, but with the (weaker) pseudo-metric*

$$\tilde{d}_k(\eta, \xi) = c_0(k) \mathbb{E} \left[ \mathbf{1}_{\{n \geq k\}} (|\text{proj}_V(M_{t_i}) \odot (\eta_{t_k-} - \xi_{t_k-})| + |\text{proj}_V(M_{t_i}) \odot (\eta_{t_k} - \xi_{t_k})|) \right]$$

*instead of the pseudo-metric  $d_k$ .*

*Proof.* Revisiting the proof of Theorem 4.3, it is apparent that this condition of Assumption 1 is only needed to remove  $\text{proj}_V(M_{t_i})$  from the expectation (see Equation (9)).  $\square$

## 5 Examples Satisfying the Assumptions

In the following, we provide examples for which we show that our assumptions of Section 2.3 are satisfied. In Section 5.1 we introduce a class of parameter filtering examples, where it is easy to verify the assumptions. Additionally, in Section 5.2 we recall the Brownian motion filtering example Krach et al. (2022, Section 7.6), which can be adapted for the input-output setting. Online classification as a special case of predicting state space models is discussed in Section 5.3. These examples are chosen sufficiently simple to compute the ground truth conditional expectation  $\hat{V}_t = \mathbb{E}[V_t | \mathcal{A}_t]$  as a reference. However, the strength of our method is its ability to work for much more general settings, where other methods would fail.



## 5.1 Parameter Filtering

One application area for the IO NJ-ODE model are *parameter filtering* examples. Here we consider a stochastic process  $(X_t^{\alpha_t})_{t \in [0, T]}$ , whose distribution depends on unknown random parameters  $\alpha = (\alpha_t)_{t \in [0, T]}$  with values  $\mathbb{R}^{d_V}$ . We focus on the special case of parameters with time dependence given by  $\alpha_t = \alpha_0 \odot \phi(t)$ , where  $\alpha_0$  is a random variable in  $\mathbb{R}^{d_V}$  and  $\phi : [0, T] \rightarrow \mathbb{R}^{d_V}$  is a deterministic continuously differentiable function; as before,  $\odot$  is the element-wise (Hadamard) product. For any fixed choice of  $\alpha$ , the distribution of  $X^\alpha$  is fixed (and can, for example, be used for sampling). In a Bayesian-like approach, we are interested in solving the following problem. Given a (prior) distribution of the parameters  $\alpha$ , we want to infer (or filter) these parameters only from observations of the process  $X^\alpha$ . In particular, the input variables for our model are  $U = X^\alpha$  and the output variables are  $V = \alpha$ . We assume that the observation framework is independent of  $(X^\alpha, \alpha)$  and satisfies the associated assumptions. Then, the conditional expectation  $\hat{V}$  satisfies

$$\hat{V}_t = \mathbb{E}[\alpha_t | \mathcal{A}_t] = \phi(t) \mathbb{E}[\alpha_0 | \mathcal{A}_t],$$

hence, the functions  $F_j$ , are continuously differentiable in their first input-coordinate  $t$ , since  $\phi$  is so. Therefore, Assumption 3 is satisfied if  $\alpha_0$  is square integrable. Indeed, by Jensen's inequality we have

$$\begin{aligned} \mathbb{E} \left[ \frac{1}{n} \sum_{i=0}^n F_j(t_i, t_i, \tilde{U}^{\leq t_i})^2 \right] &= \mathbb{E}_{\mu_Q \times \mathbb{P}} [\mathbb{E}[|V_{\tilde{t}}|_2^2 | \mathcal{A}_{\tilde{t}}]^2] \leq \mathbb{E}_{\mu_Q \times \mathbb{P}} [|V_{\tilde{t}}|_2^2] \leq \max_{0 \leq t \leq T} (|\phi(t)|_2^2) \mathbb{E}[|\alpha_0|_2^2], \\ \mathbb{E} \left[ \int_0^T |f_j(t, \tau(t), \tilde{U}^{\leq \tau(t)})|^2 dt \right] &= \mathbb{E} \left[ \int_0^T |\phi'(t) \mathbb{E}[\alpha_0 | \mathcal{A}_{\tau(t)}]|_2^2 dt \right] \leq \max_{0 \leq t \leq T} (|\phi'(t)|_2^2) T \mathbb{E}[|\alpha_0|_2^2], \end{aligned}$$

where we used Lemma 4.2 and that a continuous function is bounded on a compact set. Additionally, Assumption 4 is satisfied for the choice of  $X$  by Cohen & Elliott (2015, Lemma 16.1.4).

### 5.1.1 Constant Parameters

In the following, we give explicit examples of parameter filtering settings, where  $\alpha$  is constant, hence,  $f_j \equiv 0$ .

Note that the distributions of the parameters can easily be altered. In the case of the Brownian motion example below, we choose a normal distribution for the drift parameter, since this allows us to derive an explicit formula for the true conditional expectation to be used as reference solution. While this would otherwise not be possible, it is important to note that our model can deal with any other distribution as long as its second moment exists.

**Example 5.1.** *We consider a scaled Brownian motion with uncertain drift, i.e., a model of the form*

$$\begin{aligned} X_t &= x_0 + \mu t + \sigma W_t, \\ \mu &\sim \mathcal{N}(a, b^2), \end{aligned} \tag{24}$$

where  $\sigma, b > 0$ ,  $a, x_0 \in \mathbb{R}$  are fixed parameters and  $W$  is a standard Brownian motion (independent of  $\mu$ ). The goal is to filter out the parameter  $\mu$  from observations of  $X$ , hence,  $U = X$  is the input variable and  $V = \mu$  the output variable of the input-output NJ-ODE model. Clearly, integrability of  $\mu$  is satisfied, hence the derivations above yield that the assumptions are satisfied.

We follow the approach in Krach et al. (2022) to compute the true conditional expectation  $\hat{V}_t = \mathbb{E}[\mu | \mathcal{A}_t]$  in this setting. For observation times  $t_1, \dots, t_k$  of the process  $X$ , let  $\tilde{W}_i := W_{t_i} - W_{t_{i-1}}$  for  $1 \leq i \leq k$ . Then

$$v := (\tilde{W}_1, \dots, \tilde{W}_k, \mu)^\top \sim N((0, \dots, 0, a)^\top, \Sigma)$$

is multivariate normally distributed, where

$$\Sigma := \text{diag}(t_1 - t_0, \dots, t_k - t_{k-1}, b^2).$$

For  $I_l \in \mathbb{R}^{k \times k}$  the lower triangular matrix with 1 entries, we can express the joint vector of (centered) observations and the target variable as multivariate normal distribution

$$(X_{t_1} - x_0, \dots, X_{t_k} - x_0, \mu)^\top = \Gamma v \sim N((t_1 a, \dots, t_k a, a)^\top, \Gamma \Sigma \Gamma^\top),$$

where

$$\Gamma := \begin{pmatrix} & t_1 \\ \sigma I & \vdots \\ & t_k \\ 0 & 1 \end{pmatrix}, \quad \text{and} \quad \Gamma \Sigma \Gamma^\top =: \tilde{\Sigma} = \begin{pmatrix} \tilde{\Sigma}_{11} & \tilde{\Sigma}_{12} \\ \tilde{\Sigma}_{21} & \tilde{\Sigma}_{22} \end{pmatrix},$$

with  $\tilde{\Sigma}_{11} \in \mathbb{R}^{k \times k}$ ,  $\tilde{\Sigma}_{12} = \tilde{\Sigma}_{21}^\top \in \mathbb{R}^{k \times 1}$  and  $\tilde{\Sigma}_{22} = b^2 \in \mathbb{R}$ . Then, [Eaton \(2007, Proposition 3.13\)](#) implies that the conditional distribution of  $(\mu | X_{t_1} = x_0, \dots, X_{t_k} = x_0)$  is again normal with mean  $\hat{\mu} := a + \tilde{\Sigma}_{21} \tilde{\Sigma}_{11}^{-1} (X_{t_1} - x_0 - t_1 a, \dots, X_{t_k} - x_0 - t_k a)^\top$  and variance  $\hat{\Sigma} := \tilde{\Sigma}_{22} - \tilde{\Sigma}_{21} \tilde{\Sigma}_{11}^{-1} \tilde{\Sigma}_{12}$ . In particular, since  $\mu_t = \mu$  is constant in time and  $x_0$  is deterministic, we have for  $t_k \leq t \leq t_{k+1}$

$$\hat{V}_t = \mathbb{E}[\mu_t | \mathcal{A}_t] = \mathbb{E}[\mu | X_{t_1}, \dots, X_{t_k}] = \hat{\mu}.$$

In the following example, no explicit formula for the conditional expectation can be derived. Therefore, we resort to two alternative approaches to derive reference solutions. First, we use a particle filter, which converges to the optimal solution as the number of particles increases. We note that in contrast to our model, full knowledge of all distributions is necessary to apply the particle filter. The second approach uses a typical financial estimator, which does not need such knowledge.

**Example 5.2.** Here we consider a geometric Brownian motion with random drift and volatility parameter, starting from  $X_0 = x_0$

$$\begin{aligned} dX_t &= \mu X_t dt + \sigma X_t dW_t, \\ \mu &\sim \mathcal{N}(a, b^2), \\ \sigma &\sim \text{Unif}([\sigma_{\min}, \sigma_{\max}]), \end{aligned} \tag{25}$$

where  $a \in \mathbb{R}$ ,  $b > 0$  and  $0 < \sigma_{\min} < \sigma_{\max}$  are fixed and  $W$  is a standard Brownian motion. The goal is to filter the parameters  $V = (\mu, \sigma)$  from observations of  $U = X$ . The integrability of  $\mu, \sigma$  implies that [Assumptions 3 and 4](#) are satisfied (cf. [Section 5.1](#)). In this case, there is no explicit form for the true conditional expectation  $\hat{V}_t = \mathbb{E}[(\mu, \sigma) | \mathcal{A}_t]$ . Instead we suggest two alternative approaches. The first one approximates the true conditional expectation via particle filtering (see e.g. [Djuric et al. \(2003\)](#)) with sequential importance sampling (SIS), which is composed of the initialization, prediction and correction step. The second one is an alternative reference parameter estimation often used in finance.

For particle filtering, the initialization of the parameters  $\mu, \sigma$  is done via their joint distribution

$$\pi_0(\mu, \sigma) = \varphi(\mu; a, b) \frac{1}{\sigma_{\max} - \sigma_{\min}} \mathbb{1}_{\sigma \in [\sigma_{\min}, \sigma_{\max}]},$$

where  $\varphi(\mu; a, b)$  is the probability density function of the normal distribution  $\mathcal{N}(a, b^2)$ . In particular,  $N_p$  particles  $(\mu^{(j)}, \sigma^{(j)})$  for  $1 \leq j \leq N_p$  are sampled from this distribution and each particle is given the equal weight  $w_0^{(j)} = \frac{1}{N_p}$ . After initialization, the prediction step is applied repeatedly until a new observation becomes available, whence the correction step is triggered. For the prediction step it is enough to note that  $\mu$  and  $\sigma$  are constant parameters, hence, the predicted distribution at any given time  $t$  remains the same as the posterior distribution from the previous step. In the correction step, the distribution is updated using Bayes' theorem with the new observation  $X_{t_i} = x_i$  at time  $t_i$ . The transition density  $p(x_i | x_{i-1}, \mu, \sigma)$  for the system [\(25\)](#) is given by

$$p(x_i | x_{i-1}, \mu, \sigma) = \frac{1}{x_i \sigma \sqrt{2\pi(t_i - t_{i-1})}} \exp \left( - \frac{\left[ \ln \left( \frac{x_i}{x_{i-1}} \right) - \left( \mu - \frac{\sigma^2}{2} \right) (t_i - t_{i-1}) \right]^2}{2\sigma^2(t_i - t_{i-1})} \right).$$

Hence, the posterior distribution is updated as  $\pi_{t_i}(\mu, \sigma) \propto p(x_i | x_{i-1}, \mu, \sigma) \pi_{t_{i-1}}(\mu, \sigma)$ , leading to the updated weights

$$\hat{w}_i^{(j)} = w_{i-1}^{(j)} p(x_i^{(j)} | x_{i-1}^{(j)}, \mu^{(j)}, \sigma^{(j)}), \quad w_i^{(j)} = \frac{\hat{w}_i^{(j)}}{\sum_{j=1}^{N_p} \hat{w}_i^{(j)}}.$$

Then, the conditional expectations are given by

$$\hat{\mu}_{t_i} = \int \mu \pi_{t_i}(\mu, \sigma) d(\mu, \sigma) \approx \sum_{j=1}^{N_p} \mu^{(j)} w_i^{(j)}, \quad \hat{\sigma}_{t_i} = \int \sigma \pi_{t_i}(\mu, \sigma) d(\mu, \sigma) \approx \sum_{j=1}^{N_p} \sigma^{(j)} w_i^{(j)}.$$

Compared to our method, which is fully data-driven, the particle filter needs knowledge of the involved distributions.

For the second approach, we can use (a generalization for irregular time steps of) the standard financial estimator of  $\mu$  and  $\sigma$  as reference (Khaled & Samia, 2010). In particular, we have  $X_{t_{i+1}} = X_{t_i} \exp((\mu - \sigma^2/2)\Delta t_i + \sigma \Delta W_i)$ , where  $\Delta t_i = t_{i+1} - t_i$  and  $\Delta W_i = W_{t_{i+1}} - W_{t_i}$ . If we assume that  $\Delta t_i \geq c$  for some constant  $c > 0$  and for all  $i \in \mathbb{N}$ , then the law of large numbers (Csörgő et al., 1983, Theorem 1) implies for  $r_i := \log(X_{t_{i+1}}/X_{t_i})$ ,

$$\hat{m}_N := \frac{1}{N} \sum_{i=1}^N \frac{r_i}{\Delta t_i} \xrightarrow[N \rightarrow \infty]{\mathbb{P}\text{-a.s.}} \mu - \sigma^2/2.$$

Moreover,  $r_i/\sqrt{\Delta t_i} - (\mu - \sigma^2/2)\sqrt{\Delta t_i} \sim N(0, \sigma^2)$ , therefore,

$$\hat{\sigma}_N^2 := \frac{1}{N} \sum_{i=1}^N (r_i/\sqrt{\Delta t_i} - \hat{m}_N \sqrt{\Delta t_i})^2 \xrightarrow[N \rightarrow \infty]{\mathbb{P}\text{-a.s.}} \sigma^2.$$

This yields the estimators for drift and diffusion  $\hat{\mu}_N := \hat{m}_N + \hat{\sigma}_N^2/2$  and  $\sqrt{\hat{\sigma}_N^2}$ , respectively. It is important to keep in mind that these estimators are not an approximation of the conditional expectation and will therefore not optimize the loss function (5).

In the previous examples, the increments of the underlying process have a normal or log-normal distribution, which are relatively easy special cases. In the case of normally distributed increments, the standard Kalman filter (which needs knowledge of the underlying distribution, as the particle filter; Kalman et al., 1960) is known to be the optimal filter, retrieving the true conditional expectation (see Appendix B).

To show that our model can also deal with nonstandard cases, we consider a Cox–Ingersoll–Ross (CIR) process in the following example, where the distribution of the increments is much more complex. Again, we use a particle filter approximating the true conditional expectation as reference solution.

**Example 5.3.** We consider a Cox–Ingersoll–Ross (CIR) process with random speed, mean and volatility parameters starting from  $X_0 = x_0$ , given by

$$\begin{aligned} dX_t &= a(b - X_t)dt + \sigma \sqrt{X_t} dW_t, \\ a &\sim \text{Unif}([a_{\min}, a_{\max}]), \\ b &\sim \text{Unif}([b_{\min}, b_{\max}]), \\ \sigma &\sim \text{Unif}([\sigma_{\min}, \sigma_{\max}]), \end{aligned} \tag{26}$$

where  $W$  is a standard Brownian motion and  $0 < a_{\min} < a_{\max}$ , and similarly for  $b$  and  $\sigma$ , are fixed. The goal is to filter  $V = (a, b, \sigma)$  from observations of  $U = X$ . Assumptions 3 and 4 are satisfied due to square-integrability of all parameter distributions (cf. Section 5.1).

We use the same particle filter approach for deriving a reference solution as in Example 5.2. The initial distribution of the parameters is

$$\pi_0(a, b, \sigma) = \mathcal{U}(a; a_{\min}, a_{\max}) \mathcal{U}(b; b_{\min}, b_{\max}) \mathcal{U}(\sigma; \sigma_{\min}, \sigma_{\max}),$$

where  $\mathcal{U}(x; u_1, u_2) = (u_2 - u_1)^{-1} \mathbb{1}_{\{x \in [u_1, u_2]\}}$  is the probability density function of the uniform distribution. Moreover, the transition density from  $X_{t_{i-1}} = x_{i-1}$  to  $X_{t_i} = x_i$  with  $\Delta_i = t_i - t_{i-1}$  is given by (Cox et al., 1985)

$$p(x_i | x_{i-1}, a, b, \sigma) = c e^{-u-v} \left(\frac{v}{u}\right)^{q/2} I_q(2\sqrt{uv}), \tag{27}$$

where

$$c = \frac{2a}{(1 - e^{-a\Delta_i})\sigma^2}, \quad q = \frac{2ab - \sigma^2}{\sigma^2}, \quad u = cx_{i-1}e^{-a\Delta_i}, \quad v = cx_i,$$

and  $I_q$  is a modified Bessel function of the first kind of order  $q$ .

### 5.1.2 Time-Dependent Parameters

Finally, we extend the last example by making one of the parameters time-dependent.

**Example 5.4.** We consider the Cox–Ingersoll–Ross (CIR) process as defined in (26), but with time dependent mean parameter

$$b_t = b_0(1 + \sin(\omega t)/2), \quad b_0 \sim \text{Unif}([b_{\min}, b_{\max}]),$$

where  $\omega \in \mathbb{R}$  is a fixed. For the particle filter, we approximate the transition density by  $p(x_i|x_{i-1}, a, b_{t_{i-1}}, \sigma)$  as in (27), i.e., by setting  $b$  to the value at the last observation.

## 5.2 Stochastic Filtering of Brownian Motion

We briefly recall the example of Krach et al. (2022, Section 7.6), adapted to the context of input-output models, that is, the observation process serves as input, while the signal process is the target output. Let  $X, W$  be two i.i.d. 1-dimensional Brownian motions, let  $\alpha \in \mathbb{R}$ , then  $X$  is the unobserved signal (output) process and  $Y := \alpha X + W$  is the observation (input) process. We follow Krach et al. (2022, Section 7.6) to derive the analytic expressions of the conditional expectations. Let  $t_i$  be the observation times and define  $v := (Y_{t_1}, \dots, Y_{t_k}, X_{t_k})^\top \sim N(0, \Sigma)$ , where  $\Sigma \in \mathbb{R}^{(k+1) \times (k+1)}$  with entries

$$\Sigma_{i,j} = \begin{cases} (\alpha^2 + 1)t_{\min(i,j)}, & \text{if } i, j \leq k \\ \alpha t_{\min(i,j)}, & \text{if } (i \leq k, j = k+1) \text{ or } (i = k+1, j \leq k) \\ t_k, & \text{if } i, j = k+1 \end{cases}.$$

If we write

$$\Sigma =: \begin{pmatrix} \Sigma_{11} & \Sigma_{12} \\ \Sigma_{21} & \Sigma_{22} \end{pmatrix},$$

where  $\Sigma_{11} \in \mathbb{R}^{k \times k}$ ,  $\Sigma_{12} = \Sigma_{21}^\top \in \mathbb{R}^{k \times 1}$  and  $\Sigma_{22} = \text{Var}(X_{t_k}) = t_k \in \mathbb{R}^{1 \times 1}$ , then the conditional distribution of  $(X_{t_k} | Y_{t_1}, \dots, Y_{t_k})$  is again normal with mean  $\hat{\mu} := \Sigma_{21}\Sigma_{11}^{-1}(Y_{t_1}, \dots, Y_{t_k})^\top$  and variance  $\hat{\Sigma} := \Sigma_{22} - \Sigma_{21}\Sigma_{11}^{-1}\Sigma_{12}$  (Eaton, 2007, Proposition 3.13). In particular, we have for any  $s > 0$  that  $\mathbb{E}[X_{t_k+s} | \mathcal{A}_{t_k}] = \hat{\mu}$ .

## 5.3 Finite State Space Models and Online Classification

The Input-Output NJ-ODE model can be applied to finite state space models (SSM) and as a special case to online classification tasks. Let  $(S_t)_{t \in [0, T]}$  be a finite SSM taking values in a state space  $\mathcal{S} := \{s_1, \dots, s_{N_S}\}$ , where  $N_S \in \mathbb{N}_{\geq 2}$  is the number of states, and assume we want to predict the state of the model given (irregular and incomplete) observation of an arbitrary feature process  $U$  that satisfies Assumption 4. Choosing the target output process  $V$  to be coordinate-wise given by the indicator functions for the different states,  $V_{t,j} := \mathbb{1}_{S_t = s_j}$ , yields the conditional expectation

$$\hat{V}_t = \mathbb{E}[V_t | \mathcal{A}_t] = (\mathbb{P}[S_t = s_j | \mathcal{A}_t])_{1 \leq j \leq N_S}.$$

Hence, training our model on the input-output system  $(U, V)$  leads to an approximation of the state probabilities  $\hat{V}$ , if  $\hat{V}$  satisfies Assumption 3. Note that  $V$  automatically satisfies the integrability assumption 4, since it is bounded by 1, and for the same reason Equation (1) of Assumption 4 can be reduced to

$$\mathbb{E} \left[ \int_0^T |f_j(t, \tau(t), \tilde{U}^{\leq \tau(t)})|^2 dt \right] < \infty.$$

Online classification is the special case where the states correspond to the different classes. Clearly, we can always reduce the dimension of  $V$  by 1 there, since  $|V_t|_1 = 1$ . The following example shows an easy case of this online classification problem based on a Brownian motion.

**Example 5.5.** Let  $U := W$  be a standard Brownian motion,  $\alpha \in \mathbb{R}$  and define  $S_t := \mathbb{1}_{W_t \geq \alpha}$  to be the state space model indicating whether the Brownian motion is larger than  $\alpha$ . Hence, this is a classification task with 2 classes such that it is enough to consider the 1-dimensional  $V := S$ . The conditional expectation of  $V$  can be computed analytically as

$$\hat{V}_t = \mathbb{P}[W_t \geq \alpha | \mathcal{A}_t] = \mathbb{P}\left[\frac{(W_t - W_{\tau(t)})}{\sqrt{t - \tau(t)}} \geq \frac{\alpha - W_{\tau(t)}}{\sqrt{t - \tau(t)}} \middle| W_{\tau(t)}\right] = 1 - \Phi\left(\frac{\alpha - w}{\sqrt{t - \tau(t)}}\right) \Bigg|_{w=W_{\tau(t)}},$$

using the properties of a Brownian motion and  $\Phi$  to be the cumulative distribution function of the standard normal distribution. Hence, it is easy to verify with the Leibniz integral rule that Assumption 3 is satisfied.

## 6 Experiments

We test the applicability of the framework on synthetic datasets with reference solutions, which were discussed in Section 5.

To measure the quality of the trained models in the synthetic examples we use the *validation loss* or the *test loss*, i.e., the loss (5) on the validation or test dataset (which should be minimized by the true conditional expectation) and the *evaluation metric* (see Krach et al., 2022, Section 8), which computes the distance between the model’s prediction and the true conditional expectation on a time grid averaged over all test samples. We report the results for the best early stopped model, selected based on the validation loss.

The code for running the experiments is available at <https://github.com/FlorianKrach/PD-NJOE> and further details about the implementation of the experiments can be found in Appendix C.

### 6.1 Scaled Brownian Motion with Uncertain Drift

We consider a scaled Brownian motion with uncertain drift, as described in Example 5.1. In particular, we set  $x_0 = 0$ ,  $\sigma = 0.2$ ,  $a = 0.05$  and  $b = 0.1$ . The model gets the (irregular) observations of  $X$  as input and tries to filter out the randomly sampled drift coefficient  $\mu$ . Additionally, we let the model predict the conditional expectation of  $\mu^2$ , which allows us to derive the conditional variance (see Krach et al., 2022, Section 5)

$$\text{Var}[\mu | \mathcal{A}_t] = \mathbb{E}[\mu^2 | \mathcal{A}_t] - \mathbb{E}[\mu | \mathcal{A}_t]^2,$$

estimating the aleatoric uncertainty. In Figure 1 we show one test sample of the dataset, where we plot the conditional mean plus/minus the conditional standard deviation (approximately corresponding to a 68% normal confidence interval). We see that the model correctly learns to predict the mean  $a$  of the distribution of  $\mu$  at  $t = 0$ , where no additional information is available, and also updates its predictions correctly when new observations of  $X$  become available. The conditional variance is slightly underestimated by the model and less accurate than the conditional expectation. The lower accuracy can be explained by the fact that the values of  $\mu^2$  are mostly smaller in magnitude than the values of  $\mu$ , implying that they are less important in the loss (due to their smaller scaling). Additionally, by plotting the standard deviation, i.e., the square root of the variance, small errors of the (small) variance predictions are scaled up. The underestimation of the variance is further discussed below in Remark 6.1. The evaluation metric (which only compares the conditional mean, not the variance) is  $1.7 \cdot 10^{-6}$ , where the validation loss (which uses the predictions of  $\mu$  and  $\mu^2$ ) of the model has the minimal value (among trained epochs) of 0.01848, close to the optimal validation loss 0.01846 of the true conditional expectation.

**Remark 6.1** (Underestimating the Variance). *Krach et al. (2022) shows that this estimator of the conditional variance is asymptotically unbiased. However, if we train our model only on a finite number of paths, our model can be slightly biased. In the case of conditional variance, our model tends to underestimate the conditional variance for the following reasons: Even if our model gave unbiased but noisy estimations of  $\mathbb{E}[\mu^2 | \mathcal{A}_t]$  and  $\mathbb{E}[\mu | \mathcal{A}_t]$ , we would tend to overestimate  $\mathbb{E}[\mu | \mathcal{A}_t]^2$  due to the strong convexity of the function  $(\cdot)^2$ . An overestimation of  $\mathbb{E}[\mu | \mathcal{A}_t]^2$  together with an unbiased estimator of  $\mathbb{E}[\mu^2 | \mathcal{A}_t]$  results in underestimating  $\text{Var}[\mu | \mathcal{A}_t] = \mathbb{E}[\mu^2 | \mathcal{A}_t] - \mathbb{E}[\mu | \mathcal{A}_t]^2$ . This bias only vanishes as the number of training paths tends to infinity.*

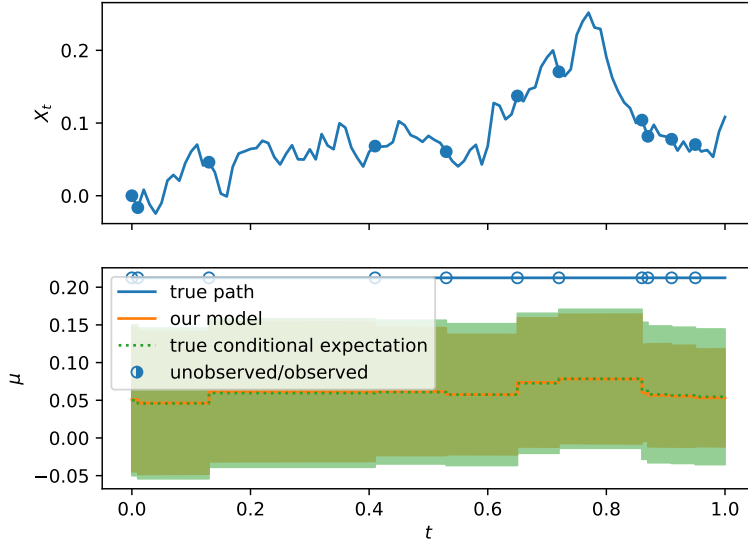


Figure 1: Predicted and true conditional expectation  $\pm$  standard deviation of the uncertain drift on a test sample of the scaled Brownian motion with random drift. The input coordinate  $U = X$  is plotted on top and the output coordinate  $V = \mu$  on the bottom. The PD-NJ-ODE replicates well the true conditional expectation of the drift.

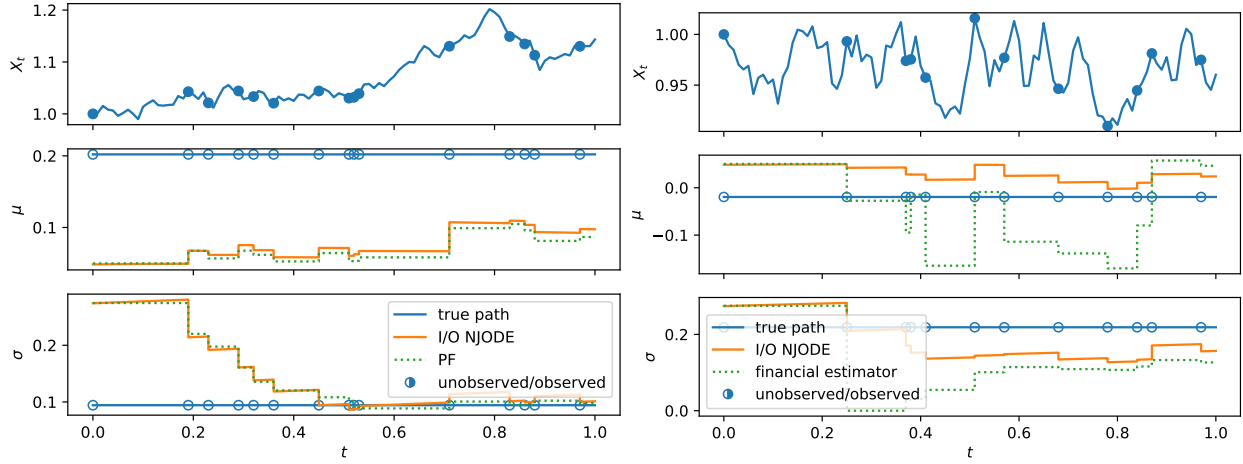


Figure 2: Predicted conditional expectation of the uncertain parameters of a geometric Brownian motion on a test sample, as well as a particle filter estimation (left) and a typical financial estimator (right) for those parameters. The input coordinate  $U = X$  is plotted on top, and the output coordinates  $V = (\mu, \sigma)$  below. As a Bayesian like estimator our model’s prediction and the particle filter have much less variance than the financial estimator.

## 6.2 Geometric Brownian Motion with Uncertain Parameters

We consider a Black–Scholes model (geometric Brownian motion) with uncertain drift and diffusion parameters, as outlined in Example 5.2. In particular, we use  $x_0 = 1$ ,  $a = 0.05$ ,  $b = 0.1$ ,  $\sigma_{\min} = 0.05$ ,  $\sigma_{\max} = 0.5$  and note that  $\Delta t_i \geq c := 0.01$  due to our sampling regime (cf. Appendix C.3). The parameters  $\mu, \sigma$  should be filtered out from the irregular observations of  $X$ .

In Figure 2 we show one sample of the test set, where we see that our model correctly learns to predict the mean of the distributions of  $\mu$  and  $\sigma$  at  $t = 0$ . Moreover, our model’s prediction closely follows the particle filter’s estimation (with 1000 particles) of the parameters. The particle filter has a slightly better minimal

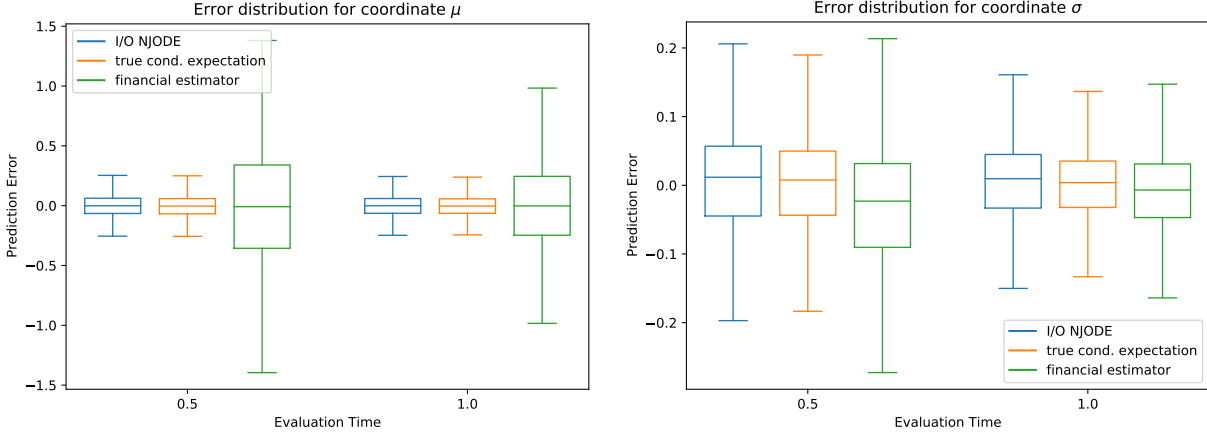


Figure 3: Distribution of prediction error of our model and reference methods at evaluation times  $t = T/2 = 0.5$  and  $t = T = 1$ .

validation loss of 0.0633 compared to 0.0652 of our model. However, it is important to keep in mind that the particle filter uses the knowledge of the distributions of  $\mu, \sigma$  and  $X$ , while our model only uses the training data. The evaluation metric on the test set at minimal validation loss<sup>3</sup> is  $2.59 \cdot 10^{-4}$ .

Compared to the financial reference log-return estimator of the parameters, our model’s prediction has less variance, since it is an approximation of the conditional expectation, which is a Bayesian-type estimator. Our model clearly outperforms the reference estimator in terms of the loss function (5), with a minimal validation loss of 0.0652 compared to 2.4674. Importantly, the reference estimator is not an approximation of the conditional expectation, which, in turn, is the unique optimizer of the loss function. Therefore, this outperformance was expected.

We compute the prediction error as the difference between the model prediction and the true value of  $\mu$  and  $\sigma$ , respectively. In Figure 3 we compare the distribution of the prediction error for our model, the particle filter approximation of the true conditional expectation and the financial estimator. The NJ-ODE and the particle filter (PF) are on par predicting the drift, with only a slight difference in the error distribution between  $T/2$  and  $T$ . The financial estimator has much larger variance (0.7 compared to 0.1 for NJ-ODE and PF), which decreases slightly from  $T/2$  to  $T$  (to 0.5). For the estimation of  $\sigma$ , the particle filter has slightly smaller variance (0.077) than the NJ-ODE model (0.080), while the financial estimator (FE) has larger variance (0.137) again. From  $T/2$  to  $T$ , the variance of all estimators decreases (to 0.061 for NJ-ODE, 0.057 for PF, 0.085 for FE), as expected, since the volatility estimation becomes more precise with the more observations available.

### 6.2.1 Empirical Convergence Study

The financial estimator should become more precise in estimating  $\sigma$  when the number of observations increases. Moreover, its estimation of  $\mu$  should improve as the time horizon  $T$  increases. In addition, the true conditional expectation should become closer to the true values of  $\mu$  and  $\sigma$ , implying that the error distributions of the NJ-ODE and the particle filter should improve. We empirically test this with a convergence study based on the Black-Scholes data model with

- the same parameters as before except for varying  $T \in \{0.1, 1, 2, 5\}$ , always keeping 100 grid points leading to increased step sizes for larger  $T$ ;
- the same parameters as before, but sampled on a grid with 1000 instead of 100 grid points, with varying observation probability  $p \in \{0.01, 0.025, 0.05, 0.1\}$  leading to an expected number of observations

<sup>3</sup>We note that the evaluation metric depends on the particle filter estimation which is random, hence, this number varies slightly between evaluations.

Table 1: Mean  $\pm$  standard deviation of the signed prediction errors for  $\mu$  and  $\sigma$  evaluated at  $t = T$  for varying values of  $T$ . This table showcases the bias and variance of each method for the predictions of both,  $\mu$  and  $\sigma$ .

	IO NJODE		Particle Filter		Financial Estimator	
$T$	$\text{err}_\mu$	$\text{err}_\sigma$	$\text{err}_\mu$	$\text{err}_\sigma$	$\text{err}_\mu$	$\text{err}_\sigma$
0.1	$0.00 \pm 0.099$	$0.00 \pm 0.07$	$0.00 \pm 0.098$	$0.00 \pm 0.06$	$-0.01 \pm 1.605$	$0.00 \pm 0.09$
1	$0.00 \pm 0.092$	$0.00 \pm 0.06$	$0.00 \pm 0.091$	$0.00 \pm 0.06$	$0.00 \pm 0.508$	$0.00 \pm 0.09$
2	$0.00 \pm 0.086$	$0.00 \pm 0.06$	$0.00 \pm 0.086$	$0.00 \pm 0.06$	$0.00 \pm 0.359$	$0.00 \pm 0.09$
5	$0.00 \pm 0.085$	$0.00 \pm 0.07$	$0.00 \pm 0.077$	$0.00 \pm 0.06$	$0.00 \pm 0.226$	$0.00 \pm 0.09$

of 10, 25, 50, 100 within  $[0, T]$ , respectively. For comparison, with the original 100 grid points and  $p = 0.1$ , we had 10 observations on average.

In Table 1 we show mean and standard deviations of the prediction errors  $\text{err}_\mu = \hat{\mu} - \mu$ , where  $\hat{\mu}$  is the model’s estimation of the true parameter  $\mu$  (which varies across samples), and similar for  $\text{err}_\sigma$ . Note that for a mean error of 0, the standard deviation of the error coincides with the (root mean square error) RMSE. We see in Table 1 that all methods produce unbiased estimates for  $\mu$  and  $\sigma$  when evaluated at  $t = T$  for varying  $T$ . The RMSE of the NJ-ODE is very close to the one of the particle filter, which approximates the true conditional expectation. For  $\mu$ , the RMSE decreases slightly for growing  $T$ . For the financial estimator, the RMSE is much larger (by a factor of 15 for  $T = 0.1$ ), however, it also decreases faster for growing  $T$  (for  $T = 5$  the factor is approximately 3). The drift is known to be difficult to estimate with the financial estimator, but, as expected, increasing the time horizon substantially improves the prediction. In contrast to this, the NJ-ODE and the PF profit in a Bayesian way from their prior knowledge (in the case of NJ-ODE learned from the training samples and in the case of PF given through knowledge of the initial distribution), while a larger time horizon  $T$  only slightly improves their predictions. The RMSE of  $\sigma$  stays approximately constant with  $T$ , since the number of observation does not change.

The results for varying observation probabilities  $p$  in Table 2 are shown when evaluating the errors at  $t = T/2 = 1/2$ . The predictions of the NJ-ODE model tend to get worse close to the time horizon  $T$ , since the model has fewer training samples there<sup>4</sup>. To avoid this (which is a side effect of the limited amount of training data), we evaluate at  $T/2$ . Again, all methods produce (nearly) unbiased estimates for  $\mu$  and  $\sigma$ . For the NJ-ODE and the particle filter, the RMSE of  $\mu$  stays approximately constant with  $p$ , while it improves for the financial estimator. This is a side-effect of the improved estimates of  $\sigma$ , since they enter into the computation of  $\hat{\mu}$  (cf. Example 5.2). The RMSE of  $\sigma$  improves for all methods with  $p$ . For the NJ-ODE the RMSE is slightly larger than for the PF. The relative difference between their RMSEs slightly grows, as the errors become smaller<sup>5</sup>. The financial estimator’s RMSE of  $\sigma$  is much larger for small  $p$  (by a factor of 2 for  $p = 0.01$ ), but also decreases faster with growing  $p$  and eventually is of the same magnitude as for the other models at  $p = 0.1$ . This shows that a large enough amount of observations can make up for the prior knowledge, hence, this prior knowledge is of less importance for the prediction of  $\sigma$  than for the prediction of  $\mu$ .

In all experiments, the evaluation metric on the test set is between  $3.8 \cdot 10^{-4}$  and  $6.5 \cdot 10^{-4}$ .

<sup>4</sup>The model’s prediction at time  $t$  only adds (indirectly) to the loss if there is an observation at  $s \geq t$ . If there is no observation afterwards, the loss is independent of this prediction, hence, minimizing the loss does not necessarily lead to an improvement of this prediction. For uniformly distributed observation times, as in this example, the probability of having an observation after  $t$  decreases with increasing  $t$ , therefore, the models predictions tend to degrade close to  $T$ .

<sup>5</sup>This can be explained by the fact that the NJ-ODE model is jointly trained to predict  $\mu$  and  $\sigma$ . As the predictions for  $\sigma$  become better, they also become less significant in the loss, which becomes increasingly dominated by the prediction error of  $\mu$ . Therefore, the model’s training focus shifts towards  $\mu$ . Training the model to only predict  $\sigma$  would avoid this issue.



Table 2: Mean  $\pm$  standard deviation of the signed prediction errors for  $\mu$  and  $\sigma$  evaluated at  $t = T/2 = 0.5$  for varying values of the observation probability  $p$ . This table showcases the bias and variance of each method for the predictions of both,  $\mu$  and  $\sigma$ .

	IO NJODE		Particle Filter		Financial Estimator	
$p$	$\text{err}_\mu$	$\text{err}_\sigma$	$\text{err}_\mu$	$\text{err}_\sigma$	$\text{err}_\mu$	$\text{err}_\sigma$
0.01	$0.00 \pm 0.10$	$0.00 \pm 0.082$	$0.00 \pm 0.10$	$0.00 \pm 0.077$	$0.02 \pm 0.99$	$-0.01 \pm 0.189$
0.025	$0.00 \pm 0.09$	$0.00 \pm 0.059$	$0.00 \pm 0.09$	$0.00 \pm 0.052$	$0.00 \pm 0.84$	$0.01 \pm 0.088$
0.05	$-0.01 \pm 0.09$	$0.00 \pm 0.045$	$0.00 \pm 0.09$	$0.00 \pm 0.038$	$-0.02 \pm 0.78$	$0.00 \pm 0.051$
0.1	$0.00 \pm 0.09$	$0.00 \pm 0.038$	$0.00 \pm 0.09$	$0.00 \pm 0.027$	$-0.02 \pm 0.70$	$0.00 \pm 0.032$

### 6.3 Cox–Ingersoll–Ross Process with Uncertain Parameters

**Experiment 1** We first consider a CIR process with constant parameters as described in Example 5.3, where we set  $x_0 = 1$ ,  $a_{\min} = 0.2$ ,  $a_{\max} = 2$ ,  $b_{\min} = 1$ ,  $b_{\max} = 5$ ,  $\sigma_{\min} = 0.05$ ,  $\sigma_{\max} = 0.5$ . While our model can easily deal with this setting, the particle filter is numerically unstable. In particular, when evaluating the transition density (27), the exponential term often becomes so small that it is numerically equal to 0, while the modified Bessel function  $I_q$  becomes so large that it is numerically equal to  $\infty$ . Whenever this happens, the density is numerically undefined and we set it to 0. If this happens for all particles, then all have the weight 0, such that we reset them to an equal weighting<sup>6</sup>. Since this happens for many of the particles, the resulting approximation of the conditional expectations is not good, as can be seen in the results. In particular, our early stopped model achieves a test loss of 1.62 compared to a test loss of 2.34 of the particle filter. In Figure 4 top left, we see that the weights of the particle filter are often reset to equal weighting, resulting in the prediction of the unconditional mean of the parameters.

**Experiment 2** To understand how well our model learns to approximate the true conditional expectation, we need a reliable reference solution to which we can compare our model. Therefore, we choose the parameter distributions in such a way that no numerical instabilities occur. In particular, the argument of  $I_q$  has to be small enough, which can be achieved through relatively large values of  $\sigma$ . However, at the same time the inequality  $2ab \geq \sigma^2$  has to be satisfied, to ensure that  $X > 0$ , since otherwise  $u$  can become 0, leading to another numerical instability in the computation of (27). To meet all requirements, we settle on the hyper-parameters  $a_{\min} = 2$ ,  $a_{\max} = 3$ ,  $b_{\min} = 1$ ,  $b_{\max} = 2$ ,  $\sigma_{\min} = 1$ ,  $\sigma_{\max} = 2$  for the parameter distributions in Example 5.3, which turn out to make the computation of the transition probability numerically stable. Hence, the particle filter can reliably be used as reference approximating the true conditional expectation. Its test loss is 0.4445, which is nearly matched by our model with a test loss of 0.4456 at the epoch of minimal validation loss. The evaluation metric is  $6.84 \cdot 10^{-4}$  there, confirming that our model approximates the true conditional expectation well, as can also be seen in Figure 4 top right.

**Experiment 3** We use Example 5.4 to show that our model can also easily deal with more complicated settings, where the parameters are not constant. In particular, we set  $w = 2\pi$  and otherwise the same parameters as in Experiment 1. Again, the particle filter is numerically unstable having an optimal test loss of 2.75, which is much larger than our model’s test loss of 1.94. In Figure 4 bottom left, we see that our model correctly picks up the time dependence of parameter  $b$ , and also that the particle filter often needs to be reset to the unconditional mean due to the numerical instability.

**Experiment 4** Finally, we use Example 5.4 with  $w = 2\pi$  and otherwise the same parameters as in Experiment 2, to get a numerically more stable particle filter as baseline (Figure 4 bottom right). As pointed out in Example 5.4, the transition probability of the particle filter is only approximated (since the

<sup>6</sup>Note that this is a way to deal with the practical issue of numerical instability, while theoretically the particle filter approach should work.

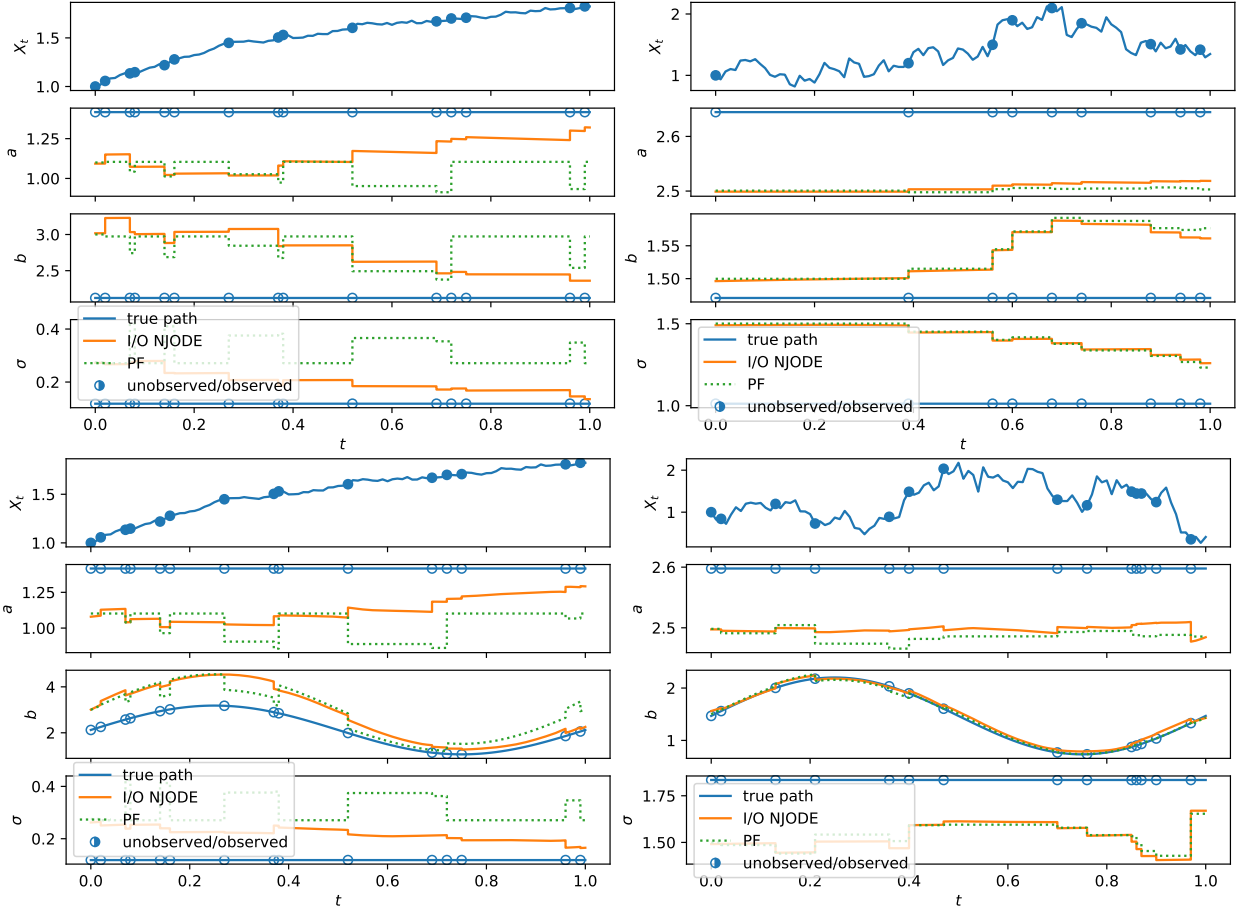


Figure 4: Test samples of parameter predictions of the CIR processes in Experiment 1 (top left), Experiment 2 (top right), Experiment 3 (bottom left) and Experiment 4 (bottom right). The input coordinate  $U = X$  is plotted on top and the output coordinates  $V = (a, b, \sigma)$  below.

time-dependent parameter  $b$  is kept constant at the value of the last observation). Hence, it is not surprising that our model achieves a smaller test loss of 0.4712 than the particle filter with 0.4745. In particular, dealing with time-dependent parameters is straight forward for our model, while the particle filter is only a non-convergent approximation of the true conditional expectation.

Overall, these experiments illustrate the flexibility and robustness of our model in contrast to the particle filter, which not only needs full knowledge of the distributions but is also numerically unstable for the CIR process except for carefully chosen parameter distributions. Moreover, our model allows for high quality approximations of the conditional expectation as can be seen in Experiment 2 and 4, where the particle filter works.

## 6.4 Brownian Motion Filtering

We consider a signal and observation process  $(X, Y)$  defined through Brownian motions as in Section 5.2 with  $\alpha = 1$ . The model uses the irregular observations of the observation process  $Y$  as input and learns to filter out the signal process  $X$ . In Figure 5 left, we see that the model learns to filter the signal process well from the observations on one sample of the test set. The minimal validation loss of the model is 0.55186 close to the optimal validation loss 0.55172 achieved by the true conditional expectation. The evaluation metric on the test set at minimal validation loss is  $9.6 \cdot 10^{-5}$ .

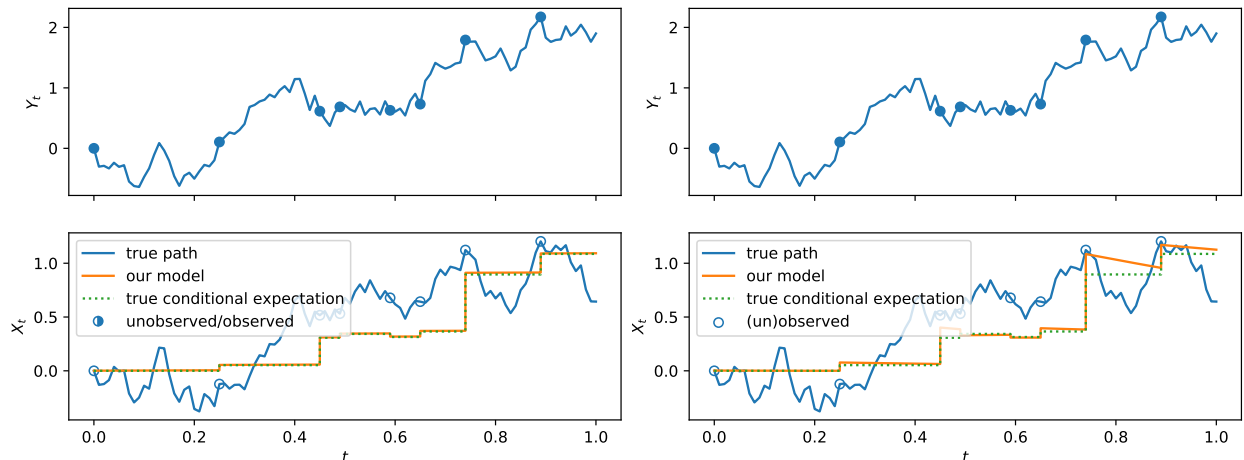


Figure 5: Predicted conditional expectation of the signal process  $X$  given the observations of the observation process  $Y$  on a test sample, as well as the true conditional expectation. The input coordinate  $U = Y$  is plotted on top, and the output coordinates  $V = X$  below. The model closely replicates the true conditional expectation when trained with the input-output objective (4) (left). Training with the old objective (28) leads to a different solution than the conditional expectation (right) as we will explain in Section 7.

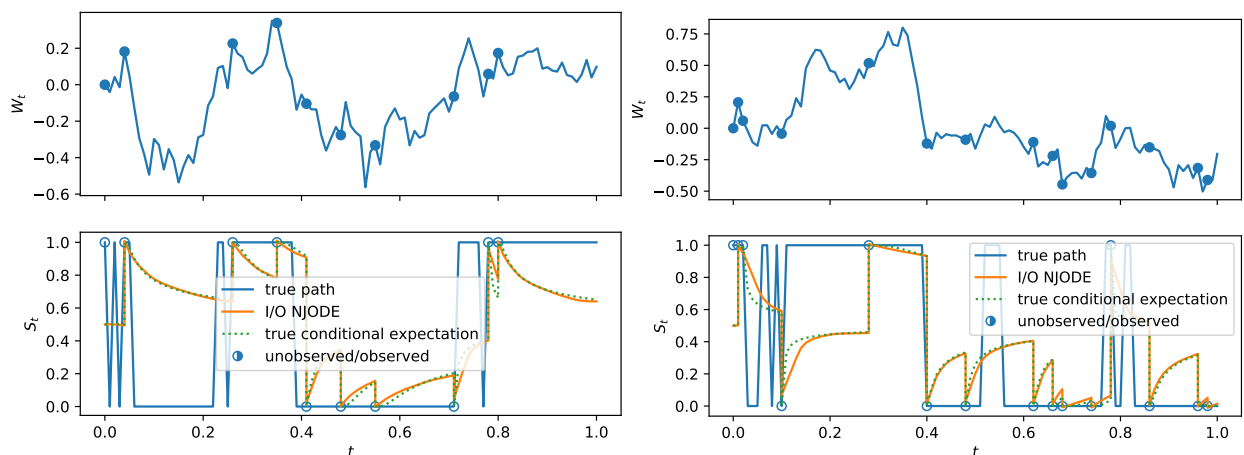


Figure 6: Predicted and true conditional probability of the input process  $U = W$  being greater than 0, by computing the conditional expectation of the output process  $V = S$  on two test samples.

## 6.5 Classifying a Brownian Motion

We consider the online classification problem described in Example 5.5 with  $\alpha = 0$ . In particular, given discrete and irregular past observations of the Brownian motion  $W$ , we want to compute the conditional probability that  $W$  is currently larger than 0. In Figure 6 we show one sample of the test set, where we see that our model replicates the true conditional probability well. At minimal validation loss, it achieves a test loss of 0.1182, which is slightly greater than the optimal test loss of 0.1147 and the evaluation metric is  $9.8 \cdot 10^{-4}$ . Examining the plots further, we see that the model does not fully learn the behavior close to the previous observation. In particular, if the previous observation was close to  $\alpha = 0$ , then the true conditional probability converges to 0.5 very quickly, while it stays longer close to 1 (or 0) if the previous observation was much larger (or smaller) than 0. To better learn this behavior, the model would need more training samples where two observations are close together, which are relatively scarce in the present setting.

## 7 Implications of the choice of Objective Function

To be able to prove the convergence results as in Krach et al. (2022) within the more general input-output setting, we had to adapt the objective function. In particular, in the input-output case (more precisely, in the case where at least one of the output variables is not itself an input variable) the minimizer of the original loss function (Krach et al., 2022, Equation 11),

$$\Psi_{\text{old}}(\eta) := \mathbb{E} \left[ \frac{1}{n} \sum_{i=1}^n (|\text{proj}_V(M_i) \odot (V_{t_i} - \eta_{t_i})|_2 + |\text{proj}_V(M_i) \odot (V_{t_i} - \eta_{t_i-})|_2)^2 \right], \quad (28)$$

is not the conditional expectation. Hence, training the NJ-ODE model with (28) should yield a solution different from the conditional expectation, with a smaller loss in terms of (28), but larger loss with respect to (4).

To intuitively understand why the optimum of the original loss function differs from the conditional expectation, consider how the squared term outside the sum in the loss function couples the two loss terms: when the second term  $|\text{proj}_V(M_i) \odot (V_{t_i} - \eta_{t_i-})|_2$  is far from zero, the first term  $|\text{proj}_V(M_i) \odot (V_{t_i} - \eta_{t_i})|_2$  becomes more significant due to the large slope of the square function. Conversely, when the second term is close to zero, the first term’s relevance diminishes (due to the diminishing slope of the square function close to zero). In the following, we consider the setting from Section 6.4 as an example. In scenarios where there is a large observed jump, we expect the unobserved process to move in the same direction to some extent, but the NJ-ODE can only respond through the first loss term. This situation creates two possible cases:

- 1) The unobserved process moves even further in the same direction, leading to a large second loss term
- 2) The unobserved process moves less in the same direction, or slightly in the opposite direction, resulting in a smaller second loss term.

The old loss function (28) tends to emphasize the first term more in Case 1, biasing the model to make larger jumps in the observed direction. Consequently, after jumping too far the model rapidly<sup>7</sup> adjusts to align with the correct conditional expectation in subsequent observations (see Figure 5 right).

In general, experimental results show that the model trained with the old loss function (28) typically outperforms the true conditional expectation when validated via (28). For instance, training the NJ-ODE with the old loss function on the same dataset as in Section 6.4 yields a test loss of 1.05132, significantly smaller than the test loss of 1.06276 achieved by the conditional expectation. This confirms that the optimum of the old loss function is different from the conditional expectation and that the NJ-ODE manages to capture this during training. On the one hand, this makes it clear that we should use the new loss (4) instead of the old one (28) when we want to learn the conditional expectation. And, on the other hand, this showcases the flexibility and powerfulness of our model, allowing it to effectively exploit subtle changes in the loss structure. Moreover, as we saw in Section 6.4, training the NJ-ODE model with the new objective function yields a very good approximation of the true conditional expectation, as our theoretical results suggest.

### 7.1 Choosing the Objective Function

In settings where the output process  $V$  is a subprocess of the input process  $U$ , i.e., when all output coordinates are also used as input coordinates (this is, in particular, the case in the setting of Krach et al., 2022), both loss functions (28) and (4) can be used. Indeed, it is easy to verify that in this case the minimizer of (28) is also given by the conditional expectation, and therefore the model converges to it with both loss functions. Hence, the question arises as to which loss function should be preferred in this case. Comparing the two objective functions, we see that the input-output (IO) loss (4) is a pure  $L^2$  objective, while the original loss (28) has an  $L^1$  aspect. In particular, by summing the two terms before squaring them, the first unsquared

<sup>7</sup>Asymptotically the model would adjust back to the true conditional expectation directly after jumping too far, but due to (implicit) regularization for any finite training time, the model takes some time to move back to the correct conditional expectation after jumping too far.

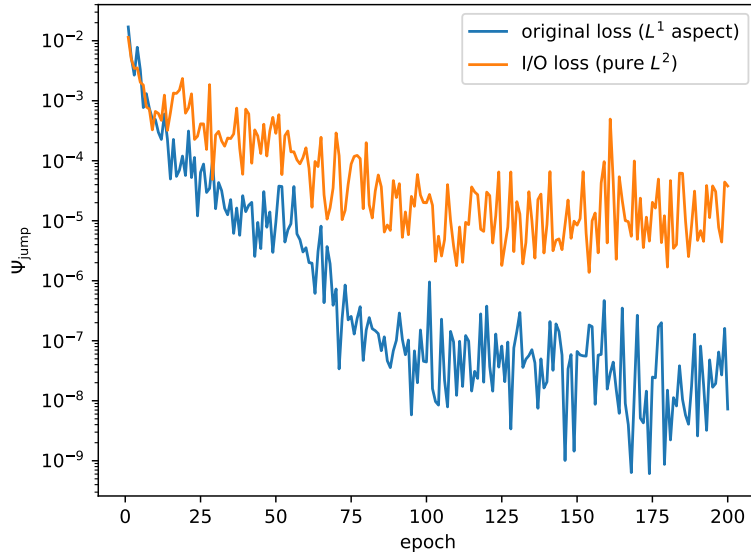


Figure 7: The jump loss  $\Psi_{\text{jump}}$  converges faster and to a smaller value when trained with the original loss function (with  $L^1$  aspect) (28) than with the pure  $L^2$  IO loss function (4).

term,  $|\text{proj}_V(M_i) \odot (V_{t_i} - \eta_{t_i})|_2$ , acts similarly as a lasso regularization. It pushes the model to perfectly and quickly learn the jump such that the first term, and therefore also the interaction term (when computing the square), vanish. On the other hand, (4) does not impose this inductive bias such that the model will only (closely) approximate, but not perfectly replicate, the jump within a finite training time (even though in the limit it would do so). In particular, the convergence will be slower.

We experimentally verify this by training the same model on the Black–Scholes dataset of [Herrera et al. \(2021, Appendix F.1\)](#) where  $U = V = X$  (cf. Appendix C.3.6) with the two different objective functions (28) and (4), while monitoring the pure *jump loss*

$$\Psi_{\text{jump}}(\eta) := \mathbb{E} \left[ \frac{1}{n} \sum_{i=1}^n |\text{proj}_V(M_i) \odot (V_{t_i} - \eta_{t_i})|_2^2 \right], \quad (29)$$

on the validation set. In particular, (29) monitors how well the model reconstructs the observation after it was fed as input. In Figure 7 we see that the model learns the jump faster and better with the original loss function. The minimal (pure jump) validation loss is  $6.1 \cdot 10^{-10}$  when training with the original loss compared to  $1.4 \cdot 10^{-6}$  when training with the IO loss. We note that a small constant  $\epsilon > 0$  is added for the computation of the square-roots in the original loss function for numerical stability. This is chosen as  $\epsilon = 10^{-10}$ , hence, this is a natural lower bound for the original loss<sup>8</sup>.

Therefore, it is beneficial to use the old loss function when both loss functions are theoretically justified, i.e., when all output coordinates are also provided as input coordinates. As soon as an output coordinate is not provided as input, the IO loss function (4) should be used to guarantee convergence to the conditional expectation.

## 8 Conclusion

In this work, we extended the framework of Neural Jump ODEs to input-output systems, making them applicable to nonparametric, data-driven filtering and classification tasks. In contrast to previous work that was limited to coinciding input and output processes, the Input-Output Neural Network Jump ODE allows for a clear separation between the observation and the estimation processes, opening the way to a variety of

<sup>8</sup>In principle, the lower bound is 0, however, during training the model does not see a benefit when decreasing this loss term further since it is overshadowed by the impact of  $\epsilon$ .

---

real-world applications where data is often incomplete and non-regular and online processing of new incoming observations is necessary for rapid decision-making.

This research combines sound theoretical contributions, providing rigorous convergence proofs that ensure the optimality of the model in an  $L^2$ -optimization framework, with an open-source ready-to-use implementation and several empirical results. Our experiments show that the IO NJ-ODE offers great flexibility and achieves high accuracy, while being simple to use as fully data-driven framework that does not need any knowledge or estimates of the underlying distributions.

With this work, we intend to open up the method of Neural Jump ODEs for promising applications in fields where input-output system dynamics play a critical role, including algorithmic finance, real-time health monitoring and system control, and risk detection in complex systems.

## Acknowledgment

The authors thank Josef Teichmann for helpful inputs and discussions. For Félix Ndonack funding is provided by the Deutsche Forschungsgemeinschaft (DFG, German Research Foundation) – Project-ID 499552394 – SFB 1597 Small Data.

## References

- William Andersson, Jakob Heiss, Florian Krach, and Josef Teichmann. Extending path-dependent NJ-ODEs to noisy observations and a dependent observation framework. *Transactions on Machine Learning Research*, 2024. ISSN 2835-8856. URL <https://openreview.net/forum?id=OT20TVCCC1>.
- Evan Archer, Il Memming Park, Lars Buesing, John Cunningham, and Liam Paninski. Black box variational inference for state space models. *arXiv preprint arXiv:1511.07367*, 2015.
- Dariusz Bugajewski and Jacek Gulgowski. On the characterization of compactness in the space of functions of bounded variation in the sense of Jordan. *Journal of Mathematical Analysis and Applications*, 484(2), 2020.
- Rich Caruana, Lorien Pratt, and Sebastian Thrun. Multitask learning. *Machine Learning 1997 28:1*, 28:41–75, 1997. ISSN 1573-0565. doi: 10.1023/A:1007379606734. URL <https://link.springer.com/article/10.1023/A:1007379606734>.
- Ilya Chevyrev and Andrey Kormilitzin. A primer on the signature method in machine learning. *arXiv*, 2016.
- Samuel N Cohen and Robert James Elliott. Stochastic calculus and applications. *Springer*, 2015.
- Adrien Corenflos, James Thornton, George Deligiannidis, and Arnaud Doucet. Differentiable particle filtering via entropy-regularized optimal transport. In *International Conference on Machine Learning*, pp. 2100–2111. PMLR, 2021.
- John C. Cox, Jonathan E. Ingersoll, and Stephen A. Ross. A theory of the term structure of interest rates. *Econometrica*, 53(2):385–407, 1985. ISSN 00129682, 14680262.
- S Csörgő, Károly Tandori, and Vilmos Totik. On the strong law of large numbers for pairwise independent random variables. *Acta Mathematica Hungarica*, 42:319–330, 1983.
- Petar M Djuric, Jayesh H Kotecha, Jianqui Zhang, Yufei Huang, Tadesse Ghirmai, Mónica F Bugallo, and Joaquin Miguez. Particle filtering. *IEEE signal processing magazine*, 20(5):19–38, 2003.
- Morris L Eaton. *Multivariate statistics: A vector space approach*. Institute of Mathematical Statistics, 2007.
- Adeline Fermanian. Embedding and learning with signatures, 2020.
- Jakob Heiss. *Inductive Bias of Neural Networks and Selected Applications*. Doctoral thesis, ETH Zurich, Zurich, 2024. URL <https://www.research-collection.ethz.ch/handle/20.500.11850/699241>.

- 
- Jakob Heiss, Josef Teichmann, and Hanna Wutte. How infinitely wide neural networks can benefit from multi-task learning - an exact macroscopic characterization. *arXiv preprint arXiv:2112.15577*, 2022. doi: 10.3929/ETHZ-B-000550890. URL <http://hdl.handle.net/20.500.11850/550890>.
- Calypto Herrera, Florian Krach, and Josef Teichmann. Neural jump ordinary differential equations: Consistent continuous-time prediction and filtering. In *International Conference on Learning Representations*, 2021. URL <https://openreview.net/forum?id=JFKR3WqwyXR>.
- Kurt Hornik. Approximation capabilities of multilayer feedforward networks. *Neural networks*, 4(2):251–257, 1991.
- Kurt Hornik, Maxwell Stinchcombe, and Halbert White. Multilayer feedforward networks are universal approximators. *Neural Networks*, 2, 1989.
- Michael I Jordan. Serial order: A parallel distributed processing approach. In *Advances in Psychology*, volume 121. Elsevier, 1997.
- Olav Kallenberg. *Foundations of modern probability*. Springer, 3rd edition, 2021.
- Rudolph Emil Kalman et al. A new approach to linear filtering and prediction problems [j]. *Journal of basic Engineering*, 82(1):35–45, 1960.
- Rajeeva L. Karandikar and B. V. Rao. *Introduction to Stochastic Calculus*. Indian Statistical Institute Series. Springer Singapore, Singapore, 2018. ISBN 978-981-10-8317-4. doi: 10.1007/978-981-10-8318-1. URL <http://link.springer.com/10.1007/978-981-10-8318-1>.
- Maximilian Karl, Maximilian Soelch, Justin Bayer, and Patrick Van der Smagt. Deep variational bayes filters: Unsupervised learning of state space models from raw data. *arXiv preprint arXiv:1605.06432*, 2016.
- Khalid Khaled and Meddahi Samia. Estimation of the parameters of the stochastic differential equations black-scholes model share price of gold. *Journal of Mathematics and Statistics*, 6(4):421, 2010.
- Franz J. Kiraly and Harald Oberhauser. Kernels for sequentially ordered data. *Journal of Machine Learning Research*, 20(31):1–45, 2019.
- Florian Krach and Josef Teichmann. Learning chaotic systems and long-term predictions with neural jump odes. *arXiv preprint arXiv:2407.18808*, 2024.
- Florian Krach, Marc Nübel, and Josef Teichmann. Optimal estimation of generic dynamics by path-dependent neural jump ODEs. *arXiv preprint arXiv:2206.14284*, 2022.
- Rahul Krishnan, Uri Shalit, and David Sontag. Structured inference networks for nonlinear state space models. In *Proceedings of the AAAI Conference on Artificial Intelligence*, volume 31, 2017.
- Rahul G Krishnan, Uri Shalit, and David Sontag. Deep kalman filters. *arXiv preprint arXiv:1511.05121*, 2015.
- Jinlin Lai, Justin Domke, and Daniel Sheldon. Variational marginal particle filters. In *International Conference on Artificial Intelligence and Statistics*, pp. 875–895. PMLR, 2022.
- Tuan Anh Le, Maximilian Igl, Tom Rainforth, Tom Jin, and Frank Wood. Auto-encoding sequential monte carlo. *arXiv*, 2017.
- Chris J Maddison, John Lawson, George Tucker, Nicolas Heess, Mohammad Norouzi, Andriy Mnih, Arnaud Doucet, and Yee Teh. Filtering variational objectives. *Advances in Neural Information Processing Systems*, 30, 2017.
- Christian Naesseth, Scott Linderman, Rajesh Ranganath, and David Blei. Variational sequential monte carlo. In *International conference on artificial intelligence and statistics*, pp. 968–977. PMLR, 2018.

Ralff. Kalman filtering: Processing all measurements together vs processing them sequentially. Mathematics Stack Exchange, 2021. URL <https://math.stackexchange.com/q/4058151>. URL: <https://math.stackexchange.com/q/4058151> (version: 2021-03-11).

Guy Revach, Nir Shlezinger, Xiaoyong Ni, Adria Lopez Escoriza, Ruud JG Van Sloun, and Yonina C Eldar. Kalmannet: Neural network aided kalman filtering for partially known dynamics. *IEEE Transactions on Signal Processing*, 70:1532–1547, 2022.

David E Rumelhart, Geoffrey E Hinton, and Ronald J Williams. Learning internal representations by error propagation. Technical report, California Univ San Diego La Jolla Inst for Cognitive Science, 1985.

## Appendix

### A Signatures

We give a brief overview of the signature transform and its universal approximation results, following [Krach et al. \(2022, Section 3.2\)](#). We start by defining paths of bounded variation.

**Definition A.1.** Let  $J$  be a closed interval in  $\mathbb{R}$  and  $d \geq 1$ . Let  $X : J \rightarrow \mathbb{R}^d$  be a path on  $J$ . The variation of  $X$  on the interval  $J$  is defined by

$$\|X\|_{var,J} = \sup_{P(J)} \sum_{t_j \in P(J)} |X_{t_j} - X_{t_{j-1}}|_2,$$

where the supremum is taken over all finite partitions  $P(J)$  of  $J$ .

**Definition A.2.** We denote the set of  $\mathbb{R}^d$ -valued paths of bounded variation on  $J$  by  $BV(J, \mathbb{R}^d)$  and endow it with the norm

$$\|X\|_{BV} := |X_0|_2 + \|X\|_{var,J}.$$

For continuous paths of bounded variation we can define the signature transform.

**Definition A.3.** Let  $J$  denote a closed interval in  $\mathbb{R}$ . Let  $X : J \rightarrow \mathbb{R}^d$  be a continuous path with finite variation. The signature of  $X$  is defined as

$$S(X) = (1, X_J^1, X_J^2, \dots),$$

where, for each  $m \geq 1$ ,

$$X_J^m = \int_{\substack{u_1 < \dots < u_m \\ u_1, \dots, u_m \in J}} dX_{u_1} \otimes \dots \otimes dX_{u_m} \in (\mathbb{R}^d)^{\otimes m}$$

is a collection of iterated integrals. The map from a path to its signature is called signature transform.

A good introduction to the signature transform with its properties and examples can be found in [Chevyrev & Kormilitzin \(2016\)](#); [Kiraly & Oberhauser \(2019\)](#); [Fermanian \(2020\)](#). In practice, we are not able to use the full (infinite) signature, but instead use a truncated version.

**Definition A.4.** Let  $J$  denote a compact interval in  $\mathbb{R}$ . Let  $X : J \rightarrow \mathbb{R}^d$  be a continuous path with finite variation. The truncated signature of  $X$  of order  $m$  is defined as

$$\pi_m(X) = (1, X_J^1, X_J^2, \dots, X_J^m),$$

i.e., the first  $m + 1$  terms (levels) of the signature of  $X$ .

Note that the size of the truncated signature depends on the dimension of  $X$ , as well as the chosen truncation level. Specifically, for a path of dimension  $d$ , the dimension of the truncated signature of order  $m$  is given by

$$\begin{cases} m + 1, & \text{if } d = 1, \\ \frac{d^{m+1} - 1}{d - 1}, & \text{if } d > 1. \end{cases} \quad (30)$$



When using the truncated signature as input to a model this results in a trade-off between accurately describing the path and model complexity.

A well-known result in stochastic analysis states that continuous functions can be uniformly approximated using truncated signatures, which is made precise in the following theorem. For references to the literature and an idea of the proof, see [Kiraly & Oberhauser \(2019\)](#), Theorem 1. This classical result was extended in in [Krach et al. \(2022, Proposition 3.8\)](#) to additionally incorporate the input  $c$  from a compact set  $C \subset \mathbb{R}^m$  which can be stated as follows:

**Proposition A.5.** *Consider  $\mathcal{P}$  as a compact subset of  $BV_0^c([0, 1], \mathcal{H})$  consisting of paths that are not tree-like equivalent, and let  $C \subset \mathbb{R}^m$  for some  $m \in \mathbb{N}$  be compact. We take the Cartesian product  $BV_0^c([0, 1], \mathcal{H}) \times \mathbb{R}^m$  with the product norm defined as the sum of the individual norms (variation norm and 1-norm). Suppose  $f : \mathcal{P} \times C \rightarrow \mathbb{R}$  is continuous. Then, for any  $\varepsilon > 0$ , there exists an  $M > 0$  and a continuous function  $\tilde{f}$  such that*

$$\sup_{(x,c) \in \mathcal{P} \times C} |f(x, c) - \tilde{f}(\pi_M(x), c)| < \varepsilon.$$

To apply this result, we need a tractable description of certain compact subsets of  $BV_0^c([0, 1], \mathbb{R}^d)$  that include suitable paths for our considerations. Since  $BV_0^c([0, 1], \mathbb{R}^d)$  is not finite dimensional, not every closed and bounded subset is compact. [Bugajewski & Gulgowski \(2020\)](#) prove in Example 4, that the following set of functions is relatively compact. As already observed in [Krach et al. \(2022, Remark 3.11\)](#) this also holds for  $\mathbb{R}^d$ -valued paths.

**Proposition A.6.** *For any  $N \in \mathbb{N}$ , the set  $A_N \subseteq BV_0^c([0, 1], \mathbb{R})$ , consisting of all piecewise linear, bounded, and continuous functions expressible as*

$$f(t) = (a_1 t) \mathbf{1}_{[s_0, s_1]}(t) + \sum_{i=2}^N (a_i t + b_i) \mathbf{1}_{(s_{i-1}, s_i]}(t),$$

*is relatively compact. Here,  $a_i, b_i \in [-N, N]$ ,  $b_1 = 0$ ,  $a_i s_i = a_{i+1} s_i + b_{i+1}$  for all  $1 \leq i \leq N$ , and  $0 = s_0 < s_1 < \dots < s_N = 1$ .*

## B Kalman Filter

If the observation and signal distributions in a filtering system are Gaussian and independent, then the Kalman filter ([Kalman et al., 1960](#)) recovers the optimal solution, i.e., the true conditional expectation. This is the case in Example 5.1, where the normally distributed drift should be filtered from observations of a Brownian motion with drift, and in the filtering example with two Brownian motions in Section 6.4.

We first recall the Kalman filter in Appendix B.1 and then show that applying it in Example 5.1 leads to the same result as the direct computation of the conditional expectation given there. The example of Section 6.4 works along the same lines.

### B.1 Definition of the Kalman Filter

The Kalman filter (without control input) assumes an underlying system of a discrete, unobserved state process  $x$  and an observation process  $z$  given as

$$x_k = F_k x_{k-1} + w_k, \quad \text{and} \quad z_k = H_k x_k + v_k, \quad (31)$$

where  $F_k$  is the state transition matrix,  $w_k \sim N(0, Q_k)$  is the process noise,  $H_k$  is the observation matrix and  $v_k \sim N(0, R_k)$  is the observation noise. The initial state  $x_0$  and all noise terms  $(w_k)_K$  and  $(v_k)_k$  are assumed to be mutually independent.

Then the Kalman filter, which is optimal in this setting, initializes the prediction of  $x$  as  $\hat{x}_{0|0} = \mathbb{E}[x_0]$  and of its covariance by  $P_{0|0} = \text{Cov}(x_0)$ . Then the Kalman filter proceeds in two steps, the prediction and the update step, which can be summarized as

$$\hat{x}_{k|k-1} = F_k \hat{x}_{k-1|k-1}, \quad P_{k|k-1} = F_k P_{k-1|k-1} F_k^\top + Q_k, \quad (\text{Predict})$$

$$\hat{x}_{k|k} = \hat{x}_{k|k-1} + K_k \tilde{y}_k, \quad P_{k|k} = (I - K_k H_k) P_{k|k-1}, \quad (\text{Update})$$

where

$$\tilde{y}_k = z_k - H_k \hat{x}_{k|k-1}, \quad S_k = H_k P_{k|k-1} H_k^\top + R_k, \quad K_k = P_{k|k-1} H_k^\top S_k^{-1}.$$

## B.2 Kalman Filter Applied to Example 5.1

There are different ways to set up the Kalman filter for the filtering task of Example 5.1, see Remark B.1. Here, we shall use the set-up resembling the computation of conditional expectation as we did it in the example. In particular, we have the constant signal process  $x_k = \mu$ , which we want to predict, hence,  $F_k = 1, w_k = 0, Q_k = 0$ , and we use only one step of the observation process, where we assume to make all observations concurrently with<sup>9</sup>

$$z_1 = (X_{t_1} - X_0, \dots, X_{t_n} - X_0)^\top = (\mu t_k + \sigma W_{t_k})_{1 \leq k \leq n}^\top,$$

hence,  $H_1 = (t_1, \dots, t_n)^\top$  and  $v_1 = (W_{t_1}, \dots, W_{t_n})^\top \sigma \sim N(0, R)$ , with  $R_{i,j} = \sigma^2 \min(t_i, t_j)$ . The initial values are  $\hat{x}_{0|0} = a$  and  $P_{0|0} = b^2$  and since the state process is constant we have  $\hat{x}_{1|0} = \hat{x}_{0|0}$  and  $P_{1|0} = P_{0|0}$ . Moreover,

$$\tilde{y}_1 = (X_{t_1} - X_0 - t_1 a, \dots, X_{t_n} - X_0 - t_n a)^\top,$$

and  $S_1 = b^2 (t_i t_j)_{i,j} + R$ . A direct calculation shows that  $S_1 = \text{Cov}(z_1)$ , which implies that  $S_1 = \tilde{\Sigma}_{11}$  holds, for  $\tilde{\Sigma}_{11}$  defined in Example 5.1. Moreover, note that  $P_{1|0} H_k^\top = b^2 (t_1, \dots, t_n) = \text{Cov}(\mu, z_1^\top) = \tilde{\Sigma}_{2,1}$ , hence,  $K_k = \tilde{\Sigma}_{2,1} \tilde{\Sigma}_{11}^{-1}$ . Therefore, the update step leads to the a posteriori prediction

$$\hat{x}_{1|1} = a + \tilde{\Sigma}_{2,1} \tilde{\Sigma}_{11}^{-1} (X_{t_1} - X_0 - t_1 a, \dots, X_{t_n} - X_0 - t_n a)^\top,$$

which coincides with the prediction  $\hat{\mu}$  computed in Example 5.1. Moreover, it is easy to verify that the a posteriori covariance satisfies  $P_{k|k} = \hat{\Sigma}$ .

**Remark B.1.** *As mentioned before, the Kalman filter could also be applied differently, leading to the same result. In particular, and probably more naturally, one could use the increments  $z_1 = (X_{t_1} - X_{t_0}, \dots, X_{t_n} - X_{t_{n-1}})$  as observations. Using them as concurrent observations, one only has to adapt  $H_1, v_1, R$  in the above computations. Checking that this coincides with the given solution in Example 5.1 might be a bit tedious. However, it is easy to adjust the computation in Example 5.1 to also use the increments, making it easy to verify that this coincides with the Kalman filter. Since the information on which is conditioned does not change whether using the increments or the values of the path  $X_{t_k}$  directly, the resulting conditional distributions, and therefore also the computed  $\hat{\mu}$ , have to coincide. Hence, all 4 mentioned ways lead to the same result. Since the increments are mutually independent, using them also allows for a multi-step (recursive) application of the Kalman filter (while this does not work with the correlated path values  $X_{t_k}$ ). It is important to note that the increments could be used as observations once at a step or multiple at a step and in arbitrary order, always leading to the same resulting estimator  $\hat{\mu}$  as was outlined, e.g., by Ralff (2021).*

## C Experimental Details

Our experiments are based on the implementation used by Krach et al. (2022), which is available at <https://github.com/FlorianKrach/PD-NJOE>. Therefore, we refer the reader to its Appendix for any details that are not provided here.

### C.1 A Practical Note on Self-Imputation

In real world settings, data is usually incomplete. In experiments, we have seen that self-imputation is an effective way to deal with missing values, outperforming imputing the last observation or 0s or only using the

<sup>9</sup>It is important not to mix up  $X_{t_k}$  and  $X_0$  which refer to the model of (24) with  $x_k$  which refer to the state process of the Kalman filter (31). For more clarity, we write here  $X_0$  (instead of  $x_0$ ) for the starting value of  $(X_t)_t$ .

---

signature as input without directly passing the current observation to the model. Using an input-output setting, where some input variables are not output variables, leads to the problem that self-imputation can not be used, since the model does not predict an estimate for all input variables. On the other hand, using all input variables also as output variables, might lead to a worsened performance, if the added input variables overshadow the actual target variables in the loss function. There are different approaches to overcome this issue.

- One can first train a separate model for predicting all input variables, and then use this model for imputation of missing values while training the second model with the actual target variables. This is probably the best possible imputation, but also the most expensive to train.
- An alternative is to jointly train both networks, and to do so efficiently, use only a different readout network  $\hat{g}_{\hat{\theta}}$  for the two models, while sharing the other neural networks  $f_{\theta}$  and  $\rho_{\theta}$ . Hence, two different losses are used to train the two models. Variants, where one of the optimizers only has access to the parameters of its respective readout network, can be used.
- Another approach is to use only one model predicting all input and the target variables at once and weighting the different variables in the loss function. Then a reasonable self-imputation and good results for the target prediction can be achieved by changing the weighting throughout the training from putting all weight on the input variables in the beginning of the training to putting all weight on the target variables later on.

We note that if a large number of training paths is available, training a different model for each output variable will usually lead to an improvement of the results, since no overshadowing of the different variables in the loss can happen. If this is of importance, then it might be beneficial to use the first approach or to use the second approach with a different readout network for each target variable.

On the other hand, if we can computationally afford to train a very large architecture with many hidden neurons for many epochs with a small learning rate but only have access to a limited number of training paths, then having one model that predicts everything could be even better in terms of generalization to new paths. If we suspect that there might be some hidden features that are valuable for predicting both the outputs and the inputs, one can even benefit from multi-task learning (Caruana et al., 1997; Heiss et al., 2022; Andersson et al., 2024; Heiss, 2024). Training one model that predicts both can help to learn more reliable features in the hidden state rather than overfitting its features to only be useful for predicting the outputs. In practice, it can still be beneficial to weight down the loss for predicting the inputs to mitigate numerical problems related to overshadowing the loss for the outputs.

## C.2 Differences between the Implementation and the Theoretical Description of the NJ-ODE

Since we use the same implementation of the PD-NJ-ODE, all differences between the implementation and the theoretical description listed in Krach et al. (2022, Appendix D.1.1) also apply here.

## C.3 Details for Synthetic Datasets

Below we list the standard settings for all synthetic datasets. Any deviations or additions are listed in the respective subsections of the specific datasets.

**Dataset.** We use the Euler scheme to sample paths from the given stochastic processes on the interval  $[0, 1]$ , i.e., with  $T = 1$  and a discretisation time grid with step size 0.01. At each time point we observe the process with probability  $p = 0.1$ . We sample between 20'000 and 100'000 paths of which 80% are used as training set and the remaining 20% as validation set. Additionally, a test set with 4'000 to 5'000 paths is generated.

**Architecture.** We use the PD-NJ-ODE with the following architecture. The latent dimension is  $d_H \in \{100, 200\}$  and all 3 neural networks have the same structure of 1 hidden layer with ReLU or tanh activation function and 100 nodes. The signature is used up to truncation level 3, the encoder is recurrent and the both the encoder and decoder use a residual connection.

---

**Training.** We use the Adam optimizer with the standard choices  $\beta = (0.9, 0.999)$ , weight decay of 0.0005 and learning rate 0.001. Moreover, a dropout rate of 0.1 is used for every layer and training is performed with a mini-batch size of 200 for 200 epochs. The PD-NJ-ODE models are trained with the loss function (4).

### C.3.1 Details for Scaled Brownian Motion with Uncertain Drift

**Dataset.** 20'000 paths are sampled for the combined training and validation set and the test set has 5'000 independent paths.

**Architecture.** We use  $d_H = 100$  and tanh activation function.

### C.3.2 Details for Geometric Brownian Motion with Uncertain Parameters

**Dataset.** 100'000 paths are sampled for the combined training and validation set and the test set has 5'000 independent paths.

**Architecture.** We use  $d_H = 100$  and ReLU activation function for the first experiments. In the convergence study we use  $d_H = 200$ .

### C.3.3 Details for CIR Process with Uncertain Parameters

**Dataset.** 100'000 paths are sampled for the combined training and validation set and the test set has 4'000 independent paths.

**Architecture.** We use  $d_H = 200$  and ReLU activation function for the first experiments. For Experiment 2, the empirical performance is slightly better when the encoder and decoder do not use residual connections (validation loss of 0.446 compared to 0.450), therefore, we report these results.

### C.3.4 Details for Brownian Motion Filtering

**Dataset.** 40'000 paths are sampled for the combined training and validation set and the test set has 4'000 independent paths.

**Architecture.** We use  $d_H = 100$  and tanh activation functions.

### C.3.5 Details for Classifying a Brownian Motion

**Dataset.** 40'000 paths are sampled for the combined training and validation set and the test set has 4'000 independent paths.

**Architecture.** We use  $d_H = 200$  and ReLU activation functions.

### C.3.6 Details for Loss Comparison on Black–Scholes

**Dataset.** The geometric Brownian motion model described in [Herrera et al. \(2021, Appendix F.1\)](#) is used with the same parameters. 20'000 paths are sampled for the combined train and validation set, no test set is used.

**Architecture.** We use  $d_H = 100$  and ReLU activation function.

## D Inductive Bias

We have proven in Theorem 4.4 that the IO NJ-ODE is asymptotically unbiased. In Sections 5 and 6, we have studied settings, where we can simulate arbitrarily many training paths. In such setting we can rely on Theorem 4.4 if we sample sufficiently many training paths. However, in settings where we observe a limited number of real-world training paths without being able to simulate further training paths, the inductive bias becomes more important. The inductive bias of NJ-ODEs has been discussed in [Andersson et al. \(2024\)](#); [Heiss \(2024\)](#) and this discussion is also applicable to IO NJ-ODE. These insights on the inductive bias can

---

be helpful for understanding when IO NJ-ODE will be able to generalize well from a few observed training paths to new unseen test paths.